Chair of Petroleum and Geothermal Energy Recovery

MONTAN UNIVERSITÄT
WWW.UNILEOBEN.AC.AT

Master Thesis

Austenite Grain Growth in a Microalloyed X80 Line Pipe Steel

Written by:
Walter Antonio / Tichauer
M00635374

Advisor:
Ernst / Gamsjäger, assoz.Prof. Dipl.-Ing. Dr.mont.

Leoben, 13.09.2017

EIDESSTATTLICHE ERKLÄRUNG

Ich erkläre an Eides statt, dass ich die vorliegende Masterarbeit selbständig und ohne fremde Hilfe verfasst, andere als die angegebenen Quellen und Hilfsmittel nicht benutzt und die den benutzten Quellen wörtlich und inhaltlich entnommenen Stellen als solche erkenntlich gemacht habe.

13.09.2017

Datum

Unterschrift Verfasser
Walter Antonio Tichauer
Matrikelnummer: 00635374

AFFIDAVIT

I hereby declare that the content of this work is my own composition and has not been submitted previously for any higher degree. All extracts have been distinguished using quoted references and all information sources have been acknowledged.

13.09.2017

Date

Author's Signature
Walter Antonio Tichauer
Matriculation number: 00635374

Danksagung / Acknowledgement

The author acknowledges the Institute of Mechanics of the Montanuniversität Leoben for the financial support and the allocation of needed instruments for this work. I am very grateful to assoz. Prof. Dipl. –Ing. Dr.mont. E. Gamsjäger for the guidance in this work as well as for valuable discussions, suggestions and most of all for the instruction in many of the subjects touched in this work. I also want to thank Ing. B. Lederhaas for the technical help when running the experiments. This work could not have been accomplished without the allocation of data from Laser Ultrasonics Technique (LUT) measurements provided by Prof. Dr Matthias Militzer and Dr. Thomas Garcin. The discussions between Prof. E. Gamsjäger, Prof. Dr Matthias Militzer, Dr. Thomas Garcin and my person were not only insightful but also very helpful.

Kurzfassung

Pipelines werden unter anderem für den Transport von Erdgas und Erdöl verwendet. Durch den Einsatz von optimierten Materialien kann die Herstellung und der Betrieb von Pipelines mit dünneren Rohrwänden und größeren Betriebsdrücken ermöglicht werden, und somit die Kosten gesenkt werden.

Die Verwendung von thermomechanisch bearbeiteten, mikrolegierten Stählen für die Herstellung von Pipelines ist weitverbreitet, wie z.B. die X80 Stahllegierung. Dieser mikrolegierte Stahl zeichnet sich durch eine Kombination von verschiedenen erforderlichen mechanischen Eigenschaften, wie z.B. hohe Festigkeit, Duktilität und sehr gute Schweißbarkeit aus. Diese Eigenschaften werden durch die Mikrostruktur des Stahls bestimmt. Die Mikrostruktur entwickelt sich während der thermomechanischen Verarbeitung des Materials und durch Schweißarbeiten. Ein Schlüsselparameter zur Beschreibung der Mikrostruktur und zur Erlangung der eben genannten Eigenschaften ist die Korngröße [1], [2]. Demzufolge ist es sowohl von wissenschaftlicher als auch von industrieller Bedeutung die Entwicklung der Korngröße und der Korngrößenverteilung im Laufe der Zeit während einer Wärmebehandlung zu bestimmen.

Typische metallographische Methoden erlauben Messungen der Korngröße erst nach dem Abschrecken der Probe auf Raumtemperatur. Neuartige experimentelle Verfahren wie High Temperature Laser Scanning Confocal Microscopy (HT-LSCM) und Laser Ultrasonics Technique (LUT) hingegen ermöglichen die in situ Beobachtung der Korngrößenentwicklung. Beide Verfahren (HT-LSCM und LUT) zeigen Vor- und Nachteile bei der Untersuchung der Korngröße. HT-LSCM ist eine Oberflächentechnik und darf somit nur verwendet werden, solange die mikroskopischen Parameter im Inneren des Körpers sich nicht zu sehr von denen an der Oberfläche unterscheiden. HT-LSCM ist eine geeignete Methode, um mikroskopische Veränderungen direkt an der Oberfläche zu charakterisieren. Die LUT-Methode liefert einen Mittelwert für die Korngröße, der nach dem Volumen gewichtet ist. Jedoch liegen dabei keinerlei Informationen über die Korngrößenverteilung vor [3].

Es ist das Ziel dieser Master Arbeit die Versuchsergebnisse beider Methoden (HT-LSCM und LUT) zu vergleichen. Es sind aussagekräftigere Ergebnisse zu erwarten als bei der Auswertung mit nur einer Methode, da beide Methoden einander ergänzen. Besonders multimodale Korngrößenverteilungen können identifiziert werden, wenn eine geeignete Auswertung der HT-LSCM Ergebnisse durchgeführt wird. Um ein besseres Verständnis der Korngrößenverteilungsentwicklung zu erlangen, wird die Kinetik des Kornwachstums analysiert.

Abstract

Pipelines are used to transport, among others, oil and gas over long distances. The use of an optimized material for the production of pipelines results in reduced costs. Smaller wall thicknesses and higher operating pressures become feasible.

Widely used base materials for these pipelines are thermomechanically treated microalloyed steels, e.g. an X-80 steel grade. It offers a combination of required mechanical properties such as high strength, ductility and excellent weldability. These properties are determined by the microstructure of the steels, which evolves during thermomechanical processing and also during welding. A key parameter to describe the microstructure and to obtain the above mentioned properties is the grain size [1], [2]. It is thus of both scientific and industrial importance to observe the evolution of the grain size and grain size distribution in time during heat treatment.

Classical metallographical methods allow to measure grain sizes only after quenching the samples to room temperature. However, the in-situ evolution of the grain sizes can be monitored by novel experimental techniques such as high temperature laser scanning confocal microscopy (HT-LSCM) and laser ultrasonics technique (LUT). Both techniques HT-LSCM and LUT have advantages and drawbacks when investigating grain growth and coarsening. HT-LSCM is a surface technique, i.e. it is only applicable to microstructures where the microstructural parameters do not alter significantly from surface near regions to the bulk material. The HT-LSCM is a powerful technique since the microstructural changes at the surface can be observed directly. LUT provides the average grain sizes in the bulk material during heat treatment; however, information about the grain size distribution is not available [3].

It is the goal of this master thesis to compare the experimental results of both techniques (i.e. HT-LSCM and LUT). It is expected that the experimental findings become more meaningful than using only one of the techniques as HT-LSCM and LUT complement each other. In particular multimodal grain size distributions can be identified by an appropriate evaluation of the HT-LSCM. In order to have a better understanding of the grain-size distribution evolution, the kinetics of grain growth will be analyzed.

Table of Content

Page

1 MOTIVATION 1

2 FUNDAMENTALS 4

2.1 Steels in general: some important aspects 4

2.2 Grain Growth 5

2.2.1 Kinetics of Grain Growth 7

2.3 Determination of the Grain Size 7

2.3.1 HT-LSCM operating principle 7

2.3.2 LUT working principle 9

2.4 Pipeline Design 10

3 EXPERIMENTAL PROCEDURE 15

3.1 HT LSCM experimental procedure 15

3.1.1 Isothermal holding 15

3.1.1.1 Resulting micrographs 16

3.1.1.2 Temperature Calculations 19

3.1.1.3 Further feedback regarding temperature calibration 21

3.1.2 Dual-stage heating 23

3.2 LUT experimental procedure 24

4 EXPERIMENTAL RESULTS 25

4.1 HT LSCM results 25

4.1.1 Grain growth during isothermal holding 25

4.1.1.1 Grain size distribution of the samples heated to 1050°C 26

4.1.1.2 Grain size distribution of the samples heated to 1150°C 28

4.1.1.3 Grain size distribution of the samples heated to 1250°C 30

4.1.2 Grain growth during dual-stage heating 31

4.2 LUT results 32

5 DISCUSSION 33

5.1 Grain-size distribution 33

5.2 Movement of triple points in grain growth 36

5.3 LUT & HT-LSCM comparison 38

6 CONCLUSION/ INTERPRETATION/ RECOMMENDATIONS 41

REFERENCES 43

LIST OF TABLES **46**

LIST OF FIGURES **47**

ABBREVIATIONS **49**

1 Motivation

Pipelines have today about 3.5 million km length all over the world and are present in over 120 countries with the objective to transport different kind of fluids. There are many projects for the construction of new pipeline networks [4].

For the transportation of oil and natural gas, pipelines are usually made of steel and vary in size from 2 to 60 inches (50.8 mm – 152.4 mm) in diameter, depending on the type of pipeline. Oil is pumped by pumping stations and gas is pressurized by compressor stations and transported at a given operating pressure-range. It has been shown that specific transportation costs decrease with increasing operating pressure [5].

Over the years, higher and higher operating pressures are used for the transportation of natural gas. With increasing operating pressures, higher loads are present in the pipeline system. Therefore, steels with improved properties are required. The use of optimized materials for the production of pipelines makes it possible to work at higher operating pressures and reduce in this way the specific transportation costs. In addition enhancing the lifetime of pipelines is positive with respect to “health security and environment (HSE)” aspects by means of decreasing the frequency and the severity of possible problems.

A better understanding of the microstructure of the material, the processes that take place in the microstructure during thermal treatment, and the relationship between the microstructure and the expected properties are required in order to manufacture line pipe steels with better mechanical properties.

When transporting oil and gas, the base material of these pipelines is austenitic steels, e.g. X-80 micro-alloyed line pipe steel. Both high strength and ductility are required for these steels as well as excellent weldability. These properties can be achieved in austenitic steels only if the grain size of the austenite grains remains small. Since the austenitic grain sizes of a region tend to grow during thermal treatment, strength and ductility of the material will be reduced [3]. Large austenite grain sizes are of particular concern in the heat-affected zone (HAZ) of a welding job.

In the past century, austenite grain sizes were measured using metallographic techniques, among others. Since then various experimental and theoretical investigations regarding grain growth are reported in literature. In this way, the state of the art regarding grain growth investigation consists with the following points:

- In classical austenite grain-growth experiments, a steel sample is heated from room temperature to a selected austenitizing temperature and held there for times that are usually much longer than the heating times. The observations made in these quasi-isothermal tests led to the introduction of the so-called grain coarsening temperature, above which significant austenite grain growth is observed [3]. Grain growth of coarse-grained austenite and the occurrence of abnormal grain growth in coarse-grained austenite have been investigated [6].

- Micro-alloying elements can be used to control the evolution of the microstructure and therefore obtain a material with the desired properties. It has been observed that the addition of micro-alloys such as V, Ti, Nb or Al can be used to prevent austenite grain growth to a certain extent [7].

- Based on experimental measurements, an analytical model was derived for predicting the austenite grain size in the HAZ [8].

- The effects of Nb on carbonitrides and its influence in austenite grain growth were analyzed [9].

- The solubility of carbides and nitrides in austenite has been studied, since the precipitation of carbonitrides showed influence in the mechanical properties of the material [10].

- A model is already proposed for the dissolution of Nb-rich precipitates [1].

- In association with the dissolution of precipitates, a criterion was developed to determine the onset and the completion of heterogeneous grain growth stages, which leads to multimodal grain size distributions [11].

- The influence of cooling rate on the precipitation behavior of carbides in microalloyed steels during continuous cooling as well as its relationship to strength has been investigated. It has been suggested that increasing the cooling rate prevents the formation of carbides [12].

- The contribution of interface precipitation on yield strength in microalloyed steels has been studied. High yield strengths are partially attributed to a high degree of nanoscale carbides interface precipitation [13].

- The influence of several combinations of Nb, Ti, and Mo complex precipitates on austenite grain-growth kinetics in a microalloyed line pipe steel has been studied in order to develop a grain growth model, which can predict the austenite grain size in the weld HAZ [1].

- A model for grain growth was developed, which includes the pinning effect of precipitates present in the steel [3]. The coarsening of the pining particles has been simulated as well [2].

- There are models, which are capable of simulating grain growth during reheating [14].

- Different models for the kinetics of a triple junction have been developed [15].

- Some efforts have been done in order to exactly determine normal and abnormal grain growth regions in austenite steels [10], [16] among others.

- By means of analyzing the grain growth behavior, an approach was developed to estimate the initial distribution of precipitates in the material and their dissolution kinetics [3].

- Different methods for estimation of the three dimensional grain size distribution based on surface measurements were developed [17].

- A method was developed to produce bimodal grain structures in low carbon steels [18].

In the meanwhile, in situ investigation of the microstructure of steels during thermal processing has become possible.

A relatively new technique is LUT. This technique allows in situ measurement of austenite grain size evolution with a time resolution of up to 50 Hz [3] making it possible to capture rapid microstructural changes, e.g. occurring during heat treatment cycles. However with this method it is, at least up to now, only possible to get the average grain size, without any information about the grain size distribution.

HT LSCM is an in situ technique, which, after evaluation, provides not only with a value for the average grain size, but with the grain size distribution as well. Because HT-LSCM is a surface technique, the results are 2D-weighted values.

The two main goals of this master thesis are:

1. To characterize the grain size distribution in a way that describes the experimental measurements accurately.
2. To compare results from the two in situ investigation methods (LUT and HT LSCM) and demonstrate, how these two methods could complement each other.

2 Fundamentals

In this section several aspects, necessary for this thesis will be discussed.

Since it is being dealt with the production of pipelines for the oil and gas industry, steels will be arranged, as they are classified in the petroleum industry. Then the microstructure of steels and its relationship to mechanical properties will be discussed. Due to this relationship, at this point the average grain size as well as the grain size distribution will become of central importance for the rest of the thesis. The HT-LSCM and LUT techniques, used for average grain-size determination, will be introduced. At the end of this chapter load scenarios present in pipeline systems and therefore the required material properties in line pipe steels will be discussed. At the same time, an insight will be gained on how material properties are linked to costs when transporting natural gas in pipeline systems.

2.1 Steels in general: some important aspects

In processing, the more familiar the engineer is with the properties of different materials, the microstructure-property relationship, and the machining of them, the easier it is going to be for him to select the appropriate material for the construction of a new product based on these criteria. Following points have to be considered for the selection of a material:

- The properties required in the new product.
- The fabrication process.

In metals, atoms are arranged in a periodic and compact way. Metallic materials are stiff, have a high ultimate tensile strength and fracture toughness, and are ductile. Since metals dispose over a big number of delocalized electrons they are good electric and thermal conductors. Some metals are magnetic, some are not.

Most metals have one of the following crystal structure [19, p. 42]:

- Face-centered cubic (fcc).
- Body-centered cubic (bcc).
- Hexagonal close packed (hcp).

In the petroleum industry, the classification of steels can be simplified as follows:

- Carbon steels
- Stainless steels
- Nickel alloys

In the steel industry in general and in the pipeline industry in particular, corrosion is one major concern. The difference between the three groups of steels aforementioned lays in the sort and amount of alloying elements to make the material corrosion-resistant. Depending on the CO_2 and H_2S partial pressures, one of these steels is going to be used, see Fig. 1. In this classification, steel alloys are included in the carbon steels group. High CO_2 partial pressures

require stainless steels, while high H_2S partial pressures require Stress Corrosion Cracking (SCC) carbon steels. In case both partial pressures are high, Ni-alloys will be required, if both partial pressures are low, carbon steels will be preferred [20].

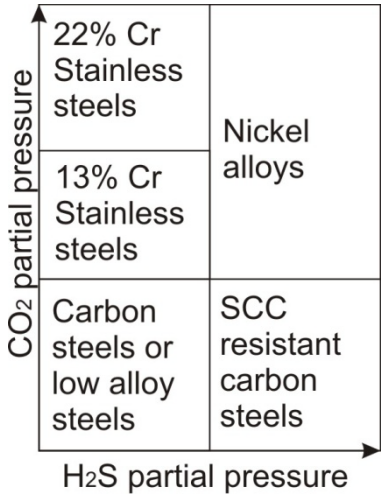

Fig. 1: Required steel type based on CO_2 and H_2S concentrations.

In pipeline systems, only carbon steels are used. The mass fraction of carbon in carbon steels is up to 2.1% by weight. As the mass fraction of carbon rises, the material strength increases as well as its hardness, nevertheless its ductility decreases [21]. In this thesis, grain growth in carbon steels will be investigated.

2.2 Grain Growth

Mechanical properties of materials such as stiffness and ductility from a fine-grained material at ambient temperature are better than the properties of coarse-grained materials [19]. That is why the average grain size, grain growth, and kinetics of grain growth will be investigated.

The regions of a material with a different crystal orientation are separated from each other by so-called grain boundaries.

Atoms in the grain boundaries are arranged in a less orderly manner. This causes also an energetic boundary. Atoms on the surface have a lower coordination number and have therefore a higher energetic level than atoms inside the grain body. In order to acquire the lowest energy level, materials tend to reduce their surface as much as possible. For example, liquids adopt the form with the smallest surface; this is the form of a sphere, as it is possible to recognize in a droplet. For solids, this is not possible due to their stiffness. The absolute value of this energy is a function of the grade of “lack of orientation” this means the energy is higher for grain boundaries, where the neighbouring grain-orientations build a bigger angle between them. Because of the grain-boundary-energy, the reactivity of the grain boundary is bigger than the one of the grains. Foreign atoms segregate preferentially in the grain-boundaries than in the grains themselves. The total surface-energy is smaller for coarse-grained than for fine-grained metals because of the less existing surface. With higher

temperatures, the grains tend to grow in order to reduce the surface energy and acquire the lowest energy level. This is the driving force for grain-growth [19].

Despite of the disordered atom-structure and the aperiodic bounds along the grain-boundaries, polycrystalline materials show a high stiffness because of cohesive forces in and around the grain-boundaries [19].

Through the movement of the grain boundaries, some grains grow at the expense of others, which at the same time shrink. It is not possible that every grain grows. In this way, the mean-grain-size increases with time, whereas at all times there is a specific grain-distribution. The movement of the grain-boundary is to be understood as a short-range diffusion of the atoms from one side of the grain-boundary to the other one. In doing so, the direction of the grain-boundary-movement is in the opposite direction than the diffusion-direction of the atoms. Since the diffusion rate increases with increasing temperature, grains are going to grow faster with higher temperatures [19].

An energetic point of view and explanation of grain growth:

> "If all grain boundaries in a polycrystal are assumed to have the same grain-boundary energy, the angles between them all should be 120°." [22, p. 129].

If a boundary is curved, a force proportional to the interfacial tension is acting toward its centre of curvature $k = \frac{1}{r}$. Therefore, the only way the boundary tension forces can balance in three dimensions is if the boundary is planar (i.e. $r \rightarrow \infty$). In a random polycrystalline aggregate, there are always boundaries with a net curvature in one direction. Consequently, a random grain structure is unstable and, on annealing at high temperatures, the unbalanced forces will cause the boundaries to migrate toward their centres of curvature. [22, p. 129]

> "If the total number of boundaries around a grain is less than six each boundary must be concave inwards. These grains will therefore shrink and eventually disappear during annealing. Larger grains, on the other hand, will have more than six boundaries and will grow. The overall result of such boundary migration is to reduce the number of grains, thereby increasing the average grain size and reducing the total grain-boundary energy." [22, p. 129]. This phenomenon is known as grain growth. It occurs at temperatures at which the grains have enough mobility. [22, p. 130].

The force on the boundary is the free energy difference per unit volume of material. [22, p. 132].

In order for an atom to be able to break away from one grain to the neighbouring grain it must acquire activation energy. [22, p. 132] In this way, the atoms vibrate with a given frequency and find accommodation in a grain with lower free energy. In real grain boundaries

not all atoms in the boundary are equivalent and some will jump more easily than others." [22, p. 134]

For a given driving force the velocity, at which boundaries move, decreases with increasing alloy content. It is worth noting that only very low concentrations of impurities are required to change the boundary mobility by orders of magnitude. "The reason for this type of behaviour arises from differences in the interactions of alloy elements or impurities with different boundaries. Generally the grain-boundary energy of a pure metal changes on alloying. Often it is reduced. Under these circumstances the concentration of alloying element in the boundary is higher than that in the matrix." [22, p. 135]

> "Not all grains will grow at the same rate: those grains which are specially oriented with respect to the matrix should have higher mobility boundaries and should overgrow the boundaries of the randomly oriented grains." [22, p. 136]

2.2.1 Kinetics of Grain Growth

During grain growth, the grain boundaries migrate reducing the total number of grains present in the material. The rate of grain growth increases rapidly with increasing temperature due to an increase in boundary mobility [22]. However, the grain-boundary migration speed is not a linear function of the driving force [22]. Particles dispersed affect grain growth and grain growth velocity. Through them grain boundaries will be caught and released depending on the driving force magnitude. At the same time, particles delimitate a final grain size no matter how much the temperature will be increased [22].

Following it will be discussed how the grain size was analyzed and the apparatus that were used.

2.3 Determination of the Grain Size

For the analysis of different properties of a material, information about the average grain-size and grain-size distribution are required. Average grain size and grain size distribution can be obtained by means of the HT-LSCM technique. The LUT results in measurements of the average grain size with excellent resolution, at different times during the experiment. Subsequently the working principle of both techniques will be discussed.

2.3.1 HT-LSCM operating principle

The samples were machined from a bar of the material in a way that they have a cylindrical geometry with a diameter of 5 mm and thickness of 2 mm. Details of the microstructure are distinguishable only if a careful preparation of the samples surface took place. For this, the sample must be firstly grinded and polished until a very smooth and mirror-like surface is obtained.

The evolution of the austenitic grains is observed in-situ under an argon atmosphere by HT-LSCM. A schematic diagram of the HT-LSCM-apparatus is presented in Fig. 2.

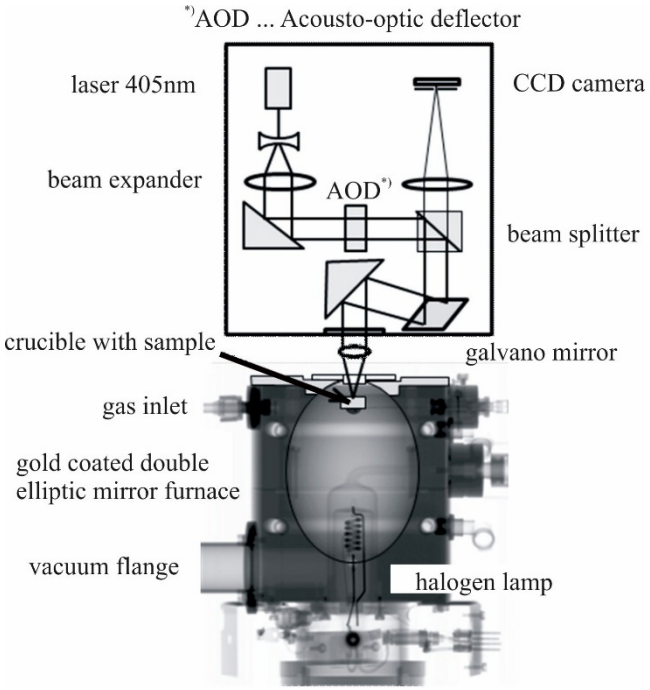

Fig. 2: Schematic set up of the HT-LSCM

By means of the halogen lamp in the lower focus, the specimen placed in the upper focus is heated inside the gold-coated double elliptic mirror furnace. Thereby it is possible to provide a defined heat treatment to the specimen. Laser light of a wavelength of 405 nm is used to illuminate the surface of the specimen. The light optical microscope will be used in reflection mode. This examination method is known as metallographic analysis.

The contrast in the images is given through differences in the reflection properties of the different structures in the microstructure. Thermal etching reveals the microstructure. The appearance of small depressions alongside the grain-boundaries of the material is known as grain grooving, see Fig. 3. The reason for this is the higher activity of the atoms in the grain-boundaries. These depressions are in the optical microscope recognizable because there, the incident light beam is going to be reflected with another angle than the light beams that are reflected from the grains [19].

In this way real time recording of dynamic processes such as grain growth is possible. In-situ micrographs are obtained for the whole duration of the experiment. By analyzing and comparing different micrographs, microstructural changes can be observed. It is possible to see how the grains grow in the obtained recordings. Actually, even the movement of the grain boundaries can be observed, if the recordings are observed in an adequate play and play back manner.

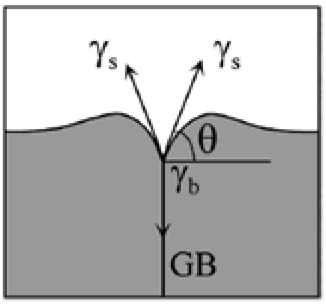

Fig. 3: Grain boundary grooving [23]

The average grain size and the distribution of grain sizes can be determined by the linear intercept method according to DIN EN ISO 643. In a micrograph, with a known magnification, that shows the structure of the grains, equidistant lines have to be placed. Subsequently the number of intersections between these lines and the grain-boundaries must be counted. The average number of intersections between line and grain-boundaries is determined. These values serve to determine the average grain size.

2.3.2 LUT working principle

The LUT is remote, continuous, and non-destructive. It can be used in situ at high temperatures to observe bulk materials and allows to measure austenite grain-growth with an acquisition rate up to 50 Hz [3].

In the LUT, ultrasonic waves are generated by a pulsed laser. As the ultrasonic sound wave propagates, it loses energy when passing through discontinuities such as grain boundaries. This results in a reduction of the amplitude of the sound wave. The unscattered sound wave is reflected back to the original surface after having travelled through the whole thickness of the sample, where it is detected by a laser interferometer [3]. Analysis of the obtained pulses provides information of the microstructure. Attenuation of the sound waves can be directly related with the grain size, as sound waves decay due to scattering by the microstructure and internal friction [3].

Fig. 4 shows schematically the experimental setup. The quantification of the grain size is based on a calibration.

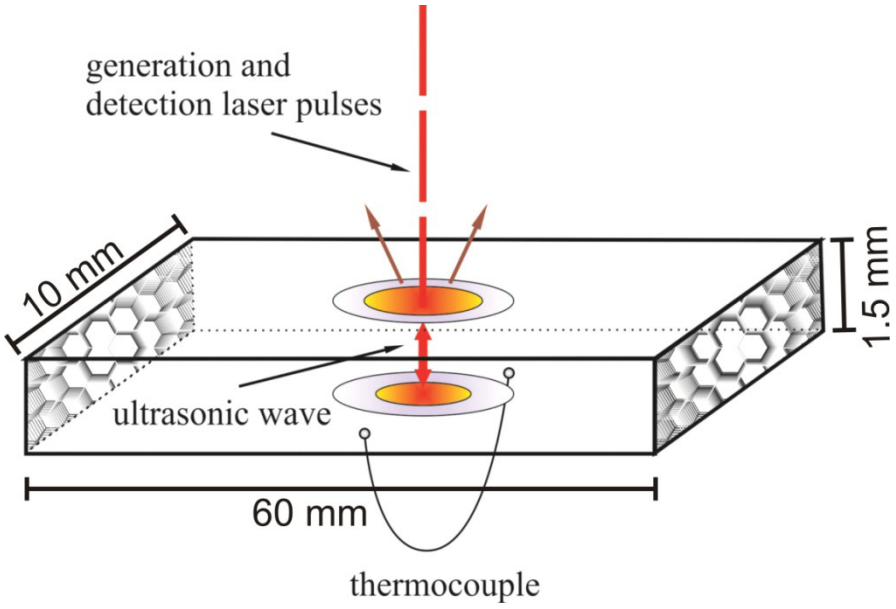

Fig. 4: Schematic diagram of the specimen geometry and the laser ultrasonics experimental set-up [3].

Accurate measurements of the average grain size and the grain size distribution are necessary for the determination of the material properties. Subsequently it will be shown how improvements of the material properties can reduce costs at a large scale.

2.4 Pipeline Design

The major activities in pipeline design are:

- Route Design: Goal is to find the best route from the starting point to the end.
- System Design: Goal is to find the optimal system for the transportation requirements.
- Optimisation: Find the most cost effective solution in terms of capital expenditure (CAPEX) and operational expenditure (OPEX).
- Permit Engineering: Obtain required permits for project implementation [24].

For the present discussion, only the system design is relevant and will be therefore considered in this chapter. In the case of gas pipelines, the system consists of the pipeline itself and compressor stations (among others such as storage and treatment facilities) arranged at certain distance intervals in order to satisfy pressure requirements. In the case of oil pipelines, pumping stations are used instead of compressor stations.

Following, different parameters that are relevant for the present loads in pipeline systems and especially for those transporting natural gas will be discussed:

- **Flow rate Q:** The flow rate is an essential parameter when dimensioning a pipeline. However, the production rate of the wells to be connected to the new pipeline system is often difficult to predict. In the same way, it is important to consider that the flow rate can change with time. For example, it makes a huge difference if the pipeline

system capacity will be increased over its lifetime or if a fixed ultimate flow rate is given [24]. It is thus desirable to design a flexible system at reasonable costs.

The type of delivery is of high importance as well. If the delivery is continuous for example, then the system can be designed with a smaller diameter as for an intermittent delivery. Designer must take regard for possible seasonal changes in gas consumption [24].

- **Velocity** v**:** Following equation relates velocity with flow rate Q and cross sectional area A: $v = \frac{Q}{A}$. Having a value for the expected flow rate, the diameter of the pipeline should be chosen based on some velocity limits. The velocity in gas lines should be less than 20 m/s in order to minimize noise, allow for corrosion inhibition and avoid erosion. In case of having corrosives present, such as CO_2, even lower velocities will be required. A minimum velocity of 3 m/s will minimize settling of liquid and solids in low spots as well as slugging [25].

- **Pressure** p**:** The required pressure head at all points along the profile can be calculated using the Bernoulli equation requiring information about altitude, friction pressure losses and required pressures at the start and the end of the pipeline system [24].

  In case that the transported medium is gas, friction pressure losses are linked to a continuous expansion of the gas along the pipeline. This expansion means a decrease in the gas density. Due to the continuity equation, the velocity of the gas is going to increase as its density decreases. This velocity increment causes on its part higher pressure losses and so on into a vicious circle. Therefore, the compression stations in a gas pipeline system have to be distributed uniformly.

  Fig. 5 shows how pressure losses increase exponentially as the velocity of the gas increases due to pressure drop.

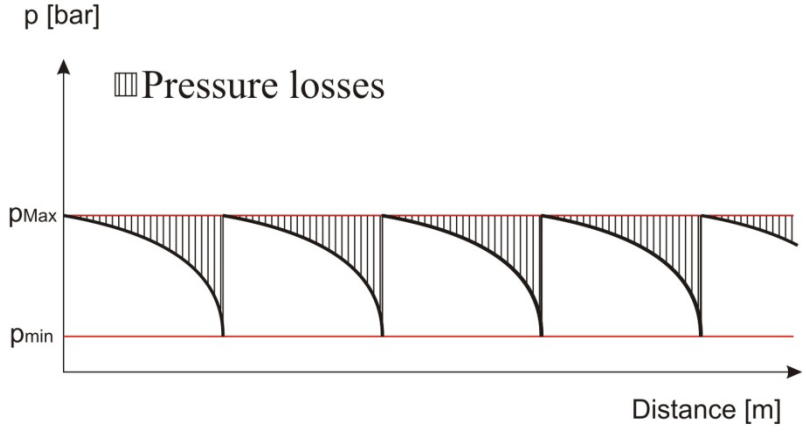

Fig. 5: Pressure losses in a gas pipeline system with four compressor stations.

The placement of compression stations is determined by the length of the pipeline, the friction pressure losses, the minimum required pressure and the maximum allowable pressure.

- **Temperature:** Piping systems subjected to temperature changes greater than 10 K, where the distance between piping turns is greater than 12 times the pipe diameter may require expansion loops [25]. Expansion loops are used to manage axial expansion and to assure that the pipeline system flexibility will accommodate expansion without building stresses in the pipes that may exceed allowable stresses.

- **Longitudinal ground profile:** The shortest path between two points is rarely the best one. High changes in altitude require compressor stations that are related to higher costs. Rough ground leads to more expensive trench excavations. Sometimes the permission for right of way through the desired areas will not be granted [24].

- **Gas composition:** In the presence of CO_2 or/and H_2S, corrosion must be avoided. This can be achieved among others by means of reducing the dew point of the gas entering the pipeline by a dehydration process [24]. Since the presence of corrosives eliminate the fatigue limit (as determined by the Wöhler curve), the use of inhibitors for corrosion prevention is standard.

By means of the boiler equation and information about the grade of the pipe, i.e. the maximum allowable stress σ_{Max}, and the dimensions of the pipe (insight diameter d), it is possible to calculate the required wall thickness t at a given operational pressure p or the maximum internal pipe pressure at the given thickness $p = \frac{2\sigma_{Max} t}{d}$.

From the boiler's equation, the proportionality between the steel grade σ_{Max} and the operating pressure p in a pipe can be clearly seen. In this way, pipeline systems built with higher steel grades allow the system to operate at higher pressures. In Fig. 6, the specific transport cost is plotted as a function of the gas-throughput. The specific transport costs are the expenditures that arise for the transport of a unit volume of a good over a unit of distance. The different curves represent different working pressures.

As it can be seen in Fig. 6, the specific transport costs decrease with increasing gas mass flow rate until a certain point. After this point, higher gas throughputs are linked with large pressure losses and therefore high-energy consumption, resulting in higher costs. With higher working pressures this vertex moves into regions of higher gas throughputs. At the same time, higher operational pressures imply lower specific transport costs for the same gas throughput within the given velocity constraints.

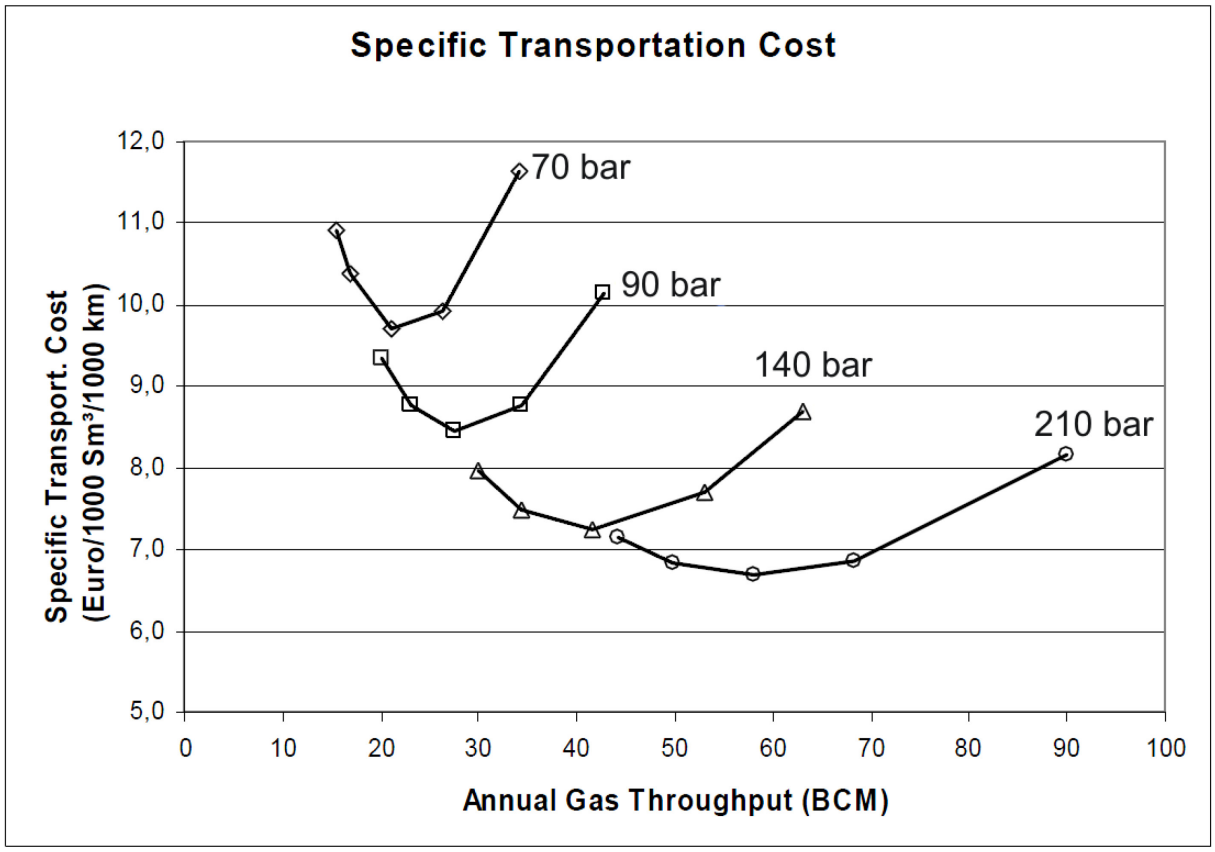

Fig. 6: Comparable Specific Transportation cost for 56" gas pipeline X80 [5]

At a given working pressure, the thickness of the line pipe steel of higher grade is lower compared to lines pipe steels of lower grade. This means saving of material. However this is limited, then if the thickness of the wall is too thin, the permitted working pressure will allow the pipe to oval. This will cause bigger stresses in the material and therefore sooner failure of the pipeline system. Therefore, in order to save costs, the use of higher operational pressures will be preferred over the production of pipelines of thinner wall thicknesses for materials of a higher grade. Due to security reasons, especially in inhabited places, a maximum operational pressure may be given by law.

In Fig. 7 and Fig. 8, the specific gas transportation cost is plotted as a function of the gas flow rate using different diameters for X70 and X80 line pipe steels respectively. As it can be seen from these two figures, lower cost are given for the X80 line pipe steel for every diameter because of the possibility of operating with higher pressures.

At a certain point the specific transportation costs for the bigger diameter pipes become lower than for the smaller pipes, because the velocity is still not too high and therefore neither the friction pressure losses nor the energy consumption.

In this case, already a difference in yield strength of 10,000 psi (i.e. 69 N/mm^2) allows an increment of the operating pressure by 50 bar. In addition, just as it has been shown in Fig. 6, higher operating pressures are linked to lower specific transportation costs at the same flow rate, as well as they shift the vertex to regions of higher gas throughputs.

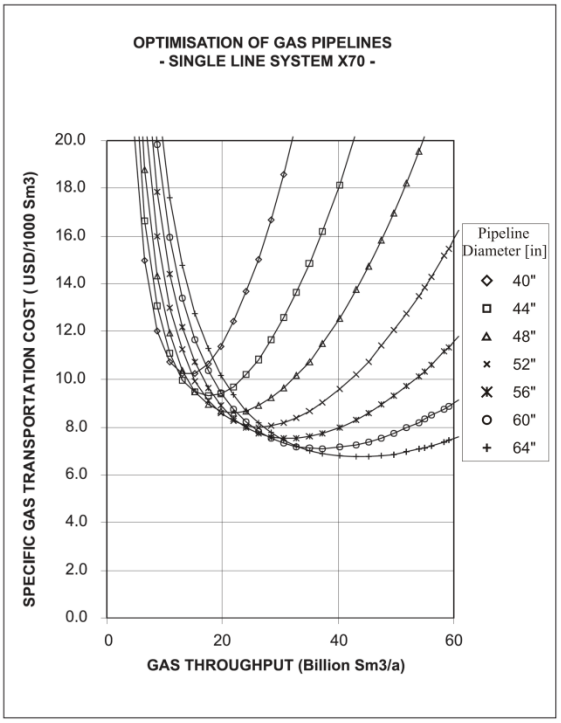

Fig. 7: Relative comparison of specific transportation cost for gas pipeline systems (steel grade X70, max. operating pressure 91 bar abs.) [26]

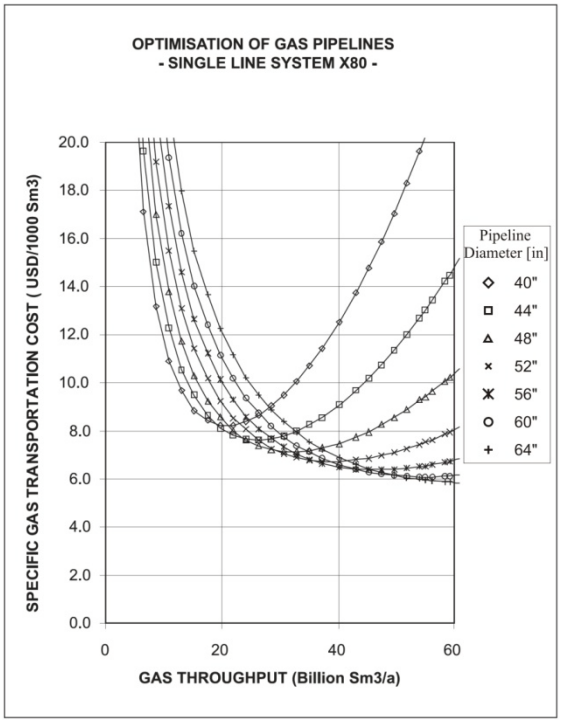

Fig. 8: Relative comparison of specific transportation cost for gas pipeline systems (steel grade X80, max. operating pressure 141 bar abs.) [26]

3 Experimental procedure

Subsequently the followed experimental procedures in both grain-size analysis methods (i.e. HT LSCM and LUT) will be described.

The samples were taken from an X80 line pipe steel containing 0.06 C, 1.65 Mn, 0.034 Nb, 0.012 Ti, 0.24 Mo, and 0.005 N in mass % as alloys.

3.1 HT LSCM experimental procedure

Experiments with two different heat treatments were performed, isothermal holding and dual-stage heating.

Selected pictures were evaluated according to the linear intercept method using the GUI of Matlab: Linecut. Standard methods for determining average grain size and grain size distribution were applied, following the ASTM norm E 112.

3.1.1 Isothermal holding

As it can be seen in Fig. 9 three heat treatments with different soak temperatures (1050°C, 1150°C, and 1250°C) were investigated. Every heat treatment was done twice for statistical evaluation; therefore, six different samples were used in total for the isothermal holding experiments.

Each one of the heating profiles consist of a heating phase, where the samples were heated at a rate of 10 Ks^{-1} to the corresponding soak temperature. Afterwards the soak temperature was hold for approximately 15 to 20 minutes. Micrographs were taken in situ during the whole length of the experiment at a rate of 15 frames per second.

At least one micrograph was analyzed for each sample. The time-temperature points marked with a star in Fig. 9 correspond to experiments that were done after a common temperature calibration the first time. From now on, they will be referred as Experiment 1. The time-temperature points marked with a circle in Fig. 9 correspond to experiments that were done after another calibration. From now on, they will be referred as Experiment 2.

Once the soak temperature is reached, the microstructure becomes more stable with time and the grain boundaries appear clearly. All micrographs selected for grain size evaluations were taken as soon as visible microstructure was given.

A clear microstructure appeared already very soon for the sample heated up to 1150°C in Experiment 2. In order to identify grain growth during the temperature-holding phase, another micrograph at a later time was evaluated as well, yellow circles in Fig. 9.

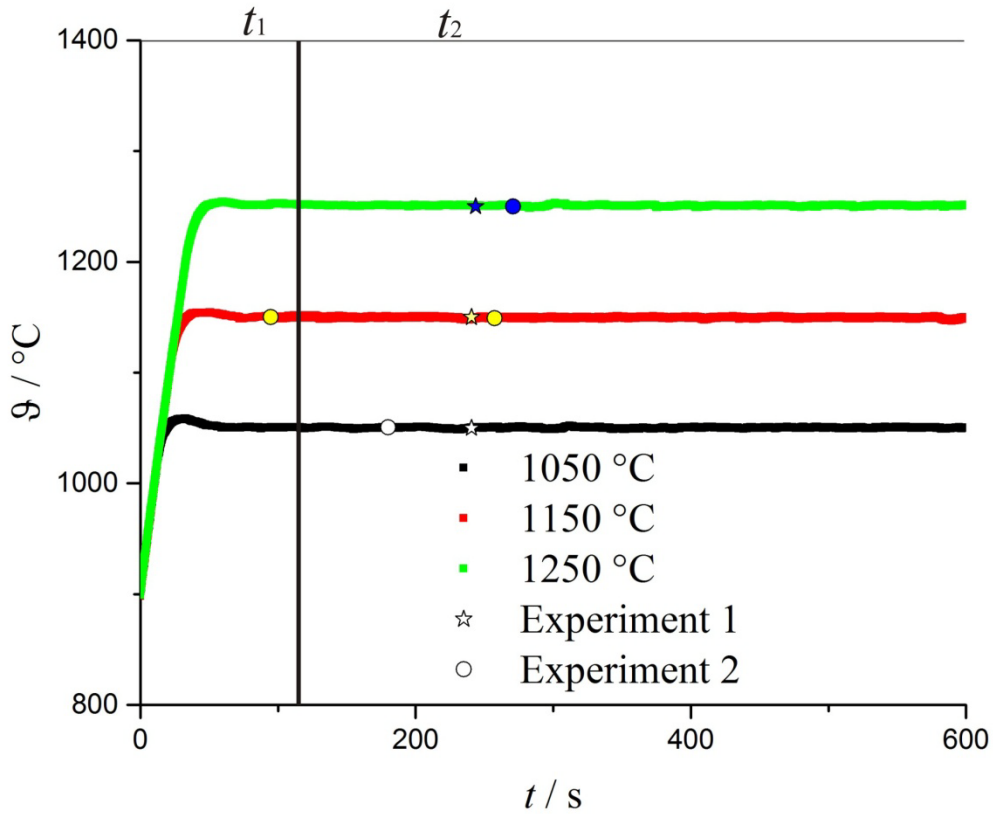

Fig. 9: Temperature profile of the samples at different soak temperatures (1050°C, 1150°C, 1250°C)

The evaluation of the selected micrographs resulted not only in an average grain size, but in a grain size distribution as well.

3.1.1.1 Resulting micrographs

During the experiments, videos of the evolving microstructures were recorded. The frame-rate was set to 15 micrographs per second. For evaluation, only micrographs of the sample after having reached the soak temperature were taken because of existing selection-criterions. These criterions state that boundaries between grains must be clear and easy to distinguish from other structures. Secondary structures, such as old boundaries must be easy to differentiate from the actual grain boundaries.

In Fig. 10 and Fig. 11, Fig. 12 and Fig. 13, and Fig. 14 and Fig. 15, micrographs of the same sample at the same temperature but at different times are shown together. Micrographs on the left are from a time as soon as possible after having reached the soak temperature with a recognizable structure. Micrographs on the right were taken long time after having reached the soak temperature, though as soon as the structure was stable and no more changes were detected with time.

The following nomenclature was used in order to characterize evaluated micrographs in their respective time-temperature coordinates in Fig. 9.

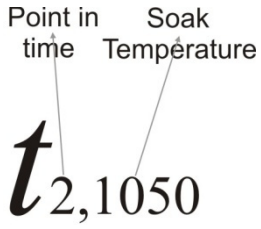

- The first subscript denotes different times. 1 if the micrograph was taken as soon as a clear structure was given and 2 if the micrograph was taken after some time passed by.
- The second subscript denotes the soak temperature.

Following micrographs are taken from Experiment 2. From these micrographs, not all were evaluated, since some of them did not satisfied visual or statistical requirements, as it will be discussed immediately.

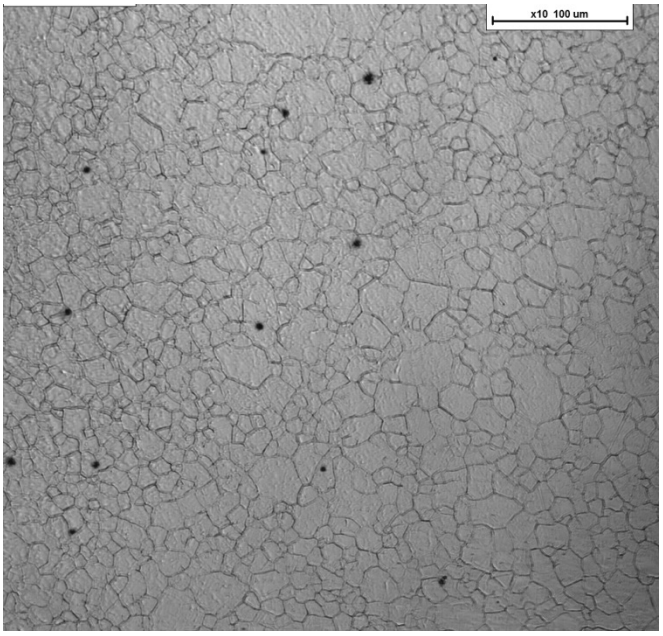

Fig. 10: Grain size distribution of the sample heated to 1050°C after $t_{1,1050}$ = 180.07 s.

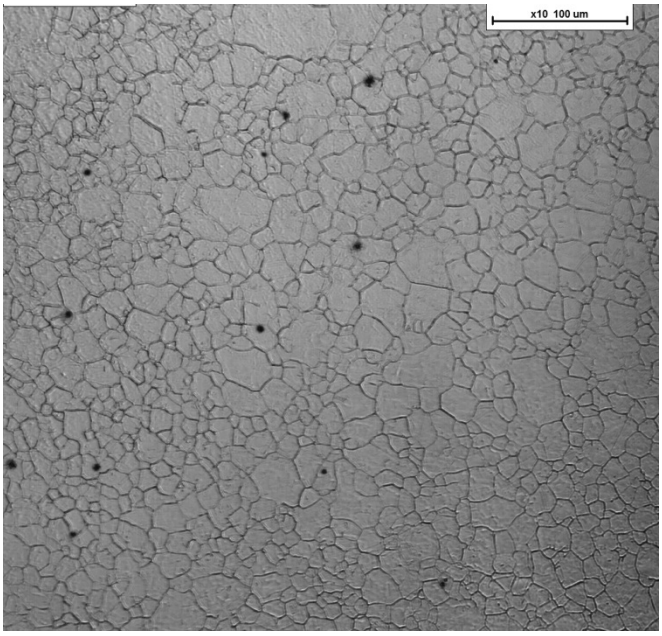

Fig. 11: Grain size distribution of the sample heated to 1050°C after $t_{2,1050}$= 242.78s.

At too early stages, after having reached the soak temperature, the grain boundaries may still be not clear enough in order to obtain meaningful results. This was the case for the micrograph in Fig. 10. Although this micrograph was evaluated, its result can only be taken as a reference for other measurements and will not be considered for further evaluation (Red numbers in Table 6). That is the reason why this micrograph cannot be found in Fig. 9.

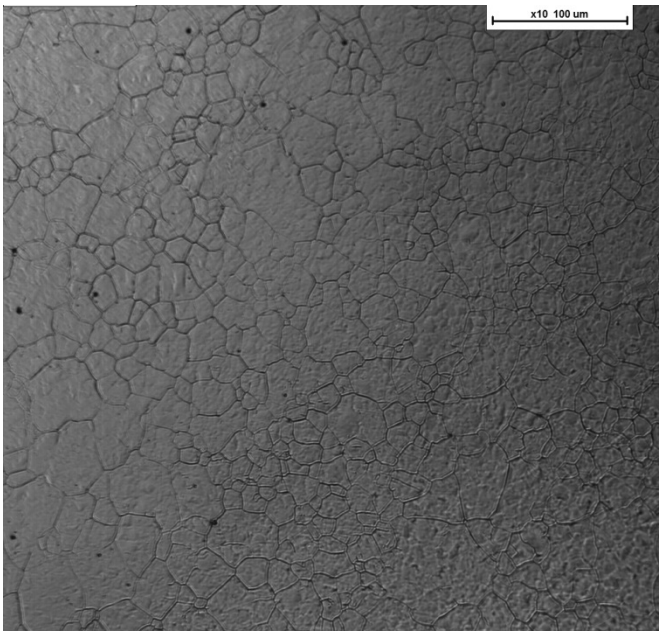

Fig. 12: Grain size distribution of the sample heated to 1150°C after $t_{1,1150}$ = 94.84 s.

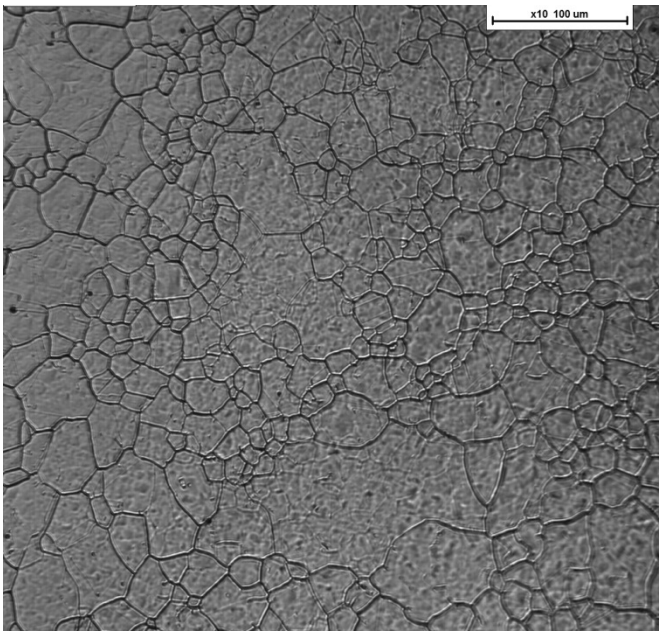

Fig. 13: Grain size distribution of the sample heated to 1150°C after $t_{2,1150}$ = 257.28 s.

The micrographs for the sample heated up to a soak temperature of 1150°C exhibit a structure that can be evaluated already at early times. The micrographs for other heat treatments did not show this aspect.

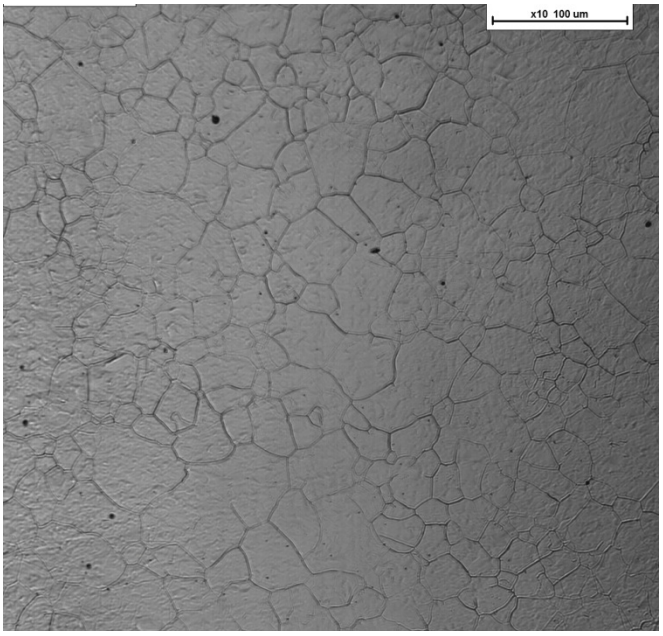

Fig. 14: Grain size distribution of the sample heated to 1250°C after t = 66.23 s.

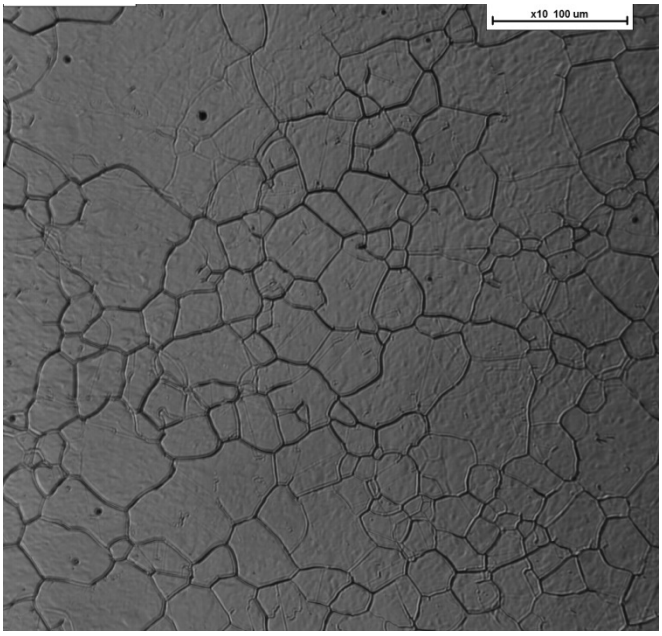

Fig. 15: Grain size distribution of the sample heated to 1250°C after t = 183.64 s.

For the determination of average grain size and grain size distribution, there are statistical requirements that demand at least 250 grains per micrograph [27]. The given micrographs in

Fig. 14 and Fig. 15 heated up to a soak temperature of 1250°C have grown so much, that too few grains are available for evaluation. A micrograph with a different magnification was used for evaluation of this sample at the given soak temperature.

From a comparison of the micrographs at different soak temperatures i.e. comparing Fig. 10, Fig. 12, and Fig. 14 or Fig. 11, Fig. 13, and Fig. 15, it is noticeable, how the average grain size augments with increasing temperature.

3.1.1.2 Temperature Calculations

Before the experiments were run, the apparatus was calibrated for oven- to sample-temperature conversions.

Calibrations are required every time a new sequence of experiments is carried out. Reason for this is the possible variation of the position of the sample holder. During each calibration, the height of the sample holder and the accuracy, with which it is positioned in the focus of the furnace, has to be corrected.

The measurements for the calibration were made using a platinum small-plate instead of an actual sample. A temperature difference was measured between this platinum small plate (100% Pt) and the Platinum-Rhodium thermoelement type R (13% Rh and 87 % Pt), upon which the samples are placed.

During calibration, the following oven vs. sample temperature data pairs were obtained:

Table 1: Oven- to sample-temperature calibration.

Experiment 1		Experiment 2	
Oven -T [K]	Sample -T [K]	Oven -T [K]	Sample -T [K]
298	317	148	152
398	416	298	302
498	520	397	393
598	614	498	495
698	706	598	589
798	797	698	679
898	888	798	767
948	926	898	858
998	977	948	906
1098	1065	998	953
1194	1150	1098	1048
1198	1153	1198	1138
1298	1243	1298	1228
1399	1331	1398	1320

These values were separated in different temperature-sectors, since the dependence of both temperatures is not linear over very large temperature ranges. In this attempt the sectors were divided in such way that there is a linear function for all oven-temperatures until reaching 900°C, which was selected as the starting point of every calculation and of the experiments (t = 0 s). Another one, which has temperature-values below and above 1050°C (the first soak-temperature) and the same for 1150°C (second soak-temperature) and 1250°C (third soak-temperature). In this way, four different oven- and sample-temperature functions were obtained.

In order to be able to convert the oven-temperature-values to sample-temperature values, it is indispensable to have the best-fit curves expressed as functions. For this, since we are dealing with linear functions ($y = mx + b$), the slope "m" and the axial intercept "b" must be determined.

Table 2: Temperature ranges for the different functions.

Experiment 1				Experiment 2			
T-range		m	b	T-range		m	b
298	898	0.95035714	39.9721429	298	898	0.93984218	20.3329777
898	1098	0.896	80.992	898	1098	0.94914286	5.86971429
1098	1198	0.88248752	96.0395175	1098	1198	0.925	30.6833333
1198	1399	0.88554833	92.596416	1198	1398	0.91	47.4866667

Table 3: Temperature conversion factors for Experiment 1.

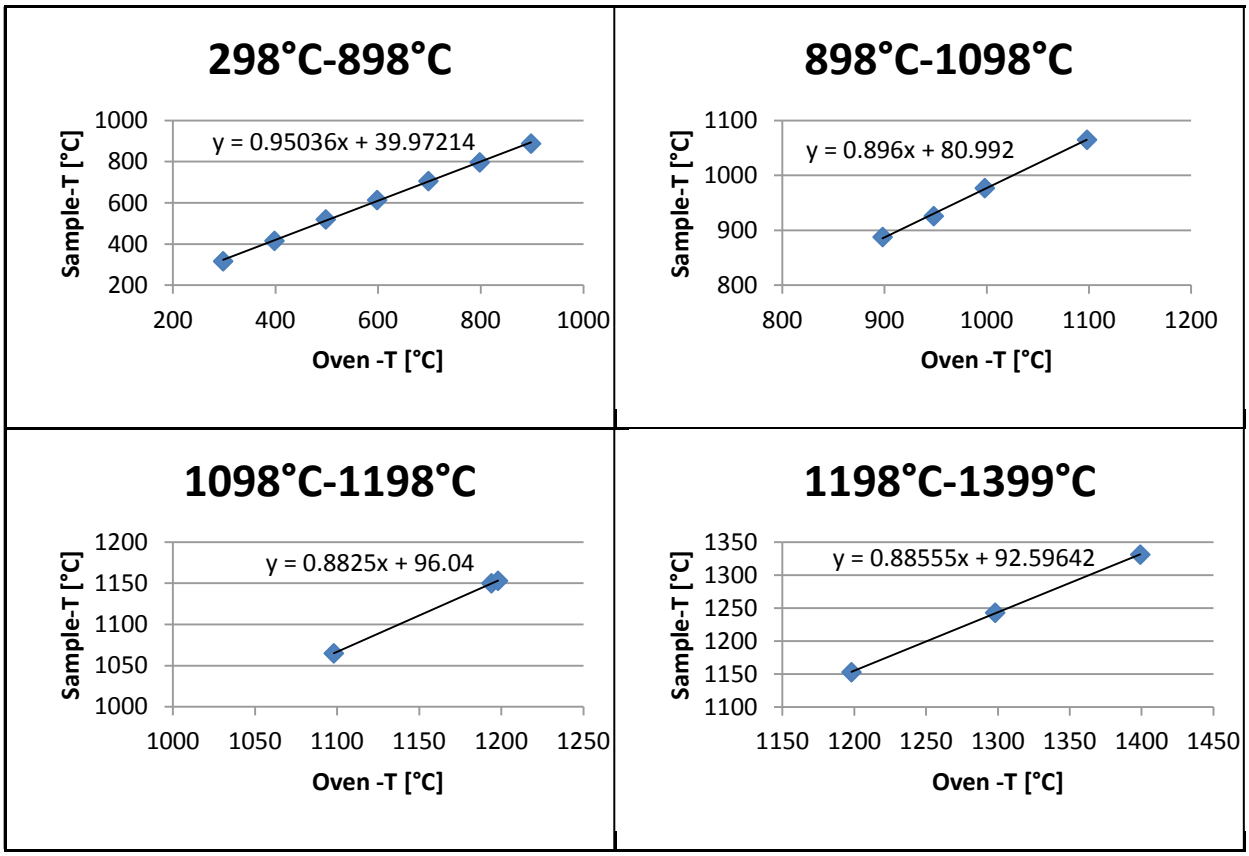

Table 4: Temperature conversion factors for Experiment 2.

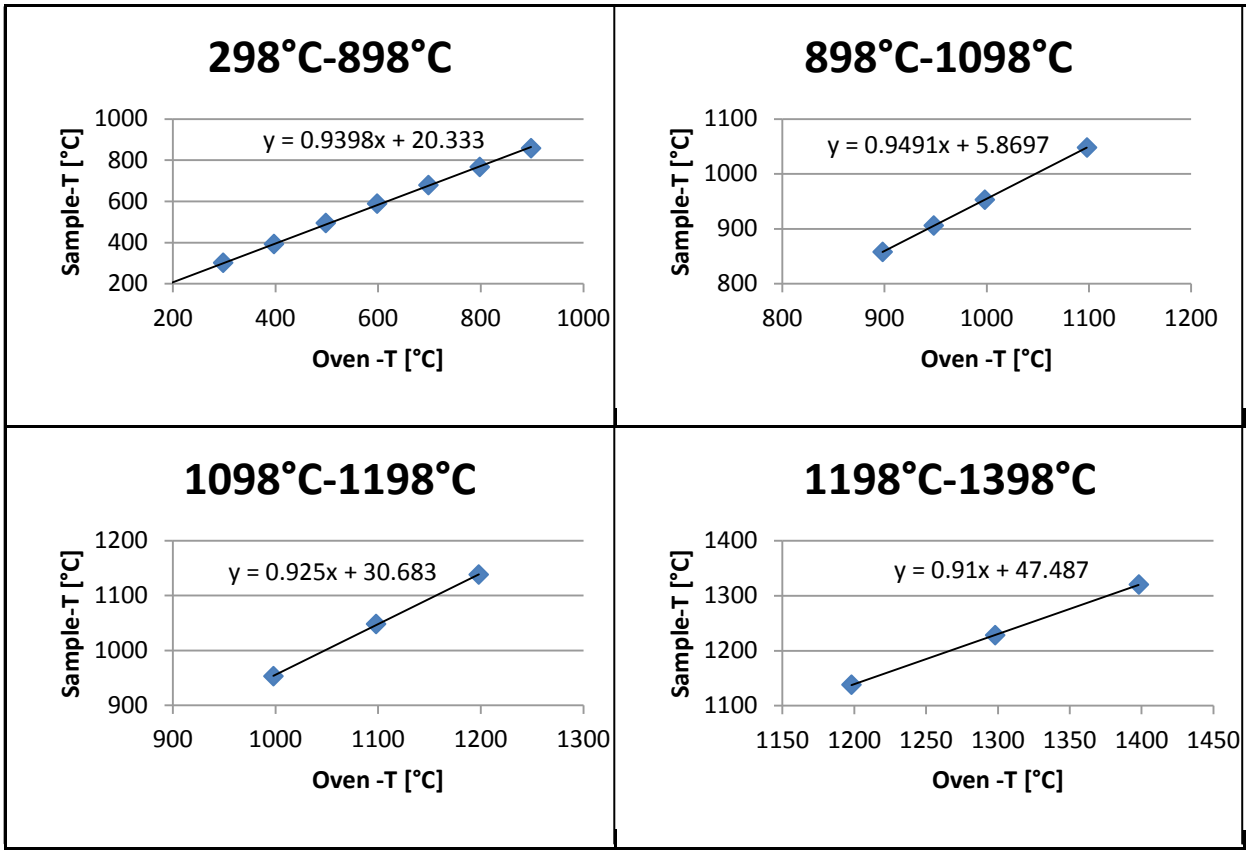

The different experiments resulted in time-oven-temperature measurements for the different micrographs. Depending on the oven-temperature that is given at a given time, this oven-temperature was converted to the sample-temperature using one of the four functions previously described. A further calibration was carried out for each experiment row (i.e. Experiment 1, Experiment 2 and Dual-stage heating). The conversion of oven-temperature to sample-temperature was automated by using If-Else-statements.

3.1.1.3 Further feedback regarding temperature calibration

As it has been discussed in 3.1.1.2 Temperature Calculations, temperature calibrations have to be done every time the setup is installed. In order to proof the reliability of the calibration, images of samples from different experiments, though heated up to the same soak temperature were compared. Since they are samples of the same material heated up to the same soak temperature, similar grain sizes are expected. Noticeable differences in the grain size for two different samples heated up to the same soak temperature would imply an inaccurate temperature-calibration procedure.

As it can be seen from following figures (i.e. Fig. 16, Fig. 17, Fig. 18, Fig. 19, Fig. 20 and Fig. 21), the grain sizes are very similar for the different samples heated up to the same soak temperature regardless of the different calibrations that took place on the apparatus. In this way, it is possible to assure the reliability of the temperature-calibrations.

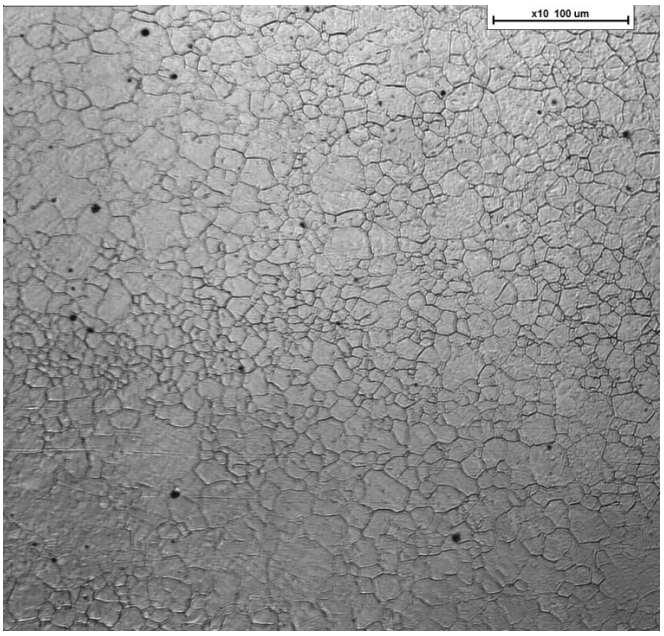

Fig. 16: Sample from Experiment 1 heated up to 1050°C.

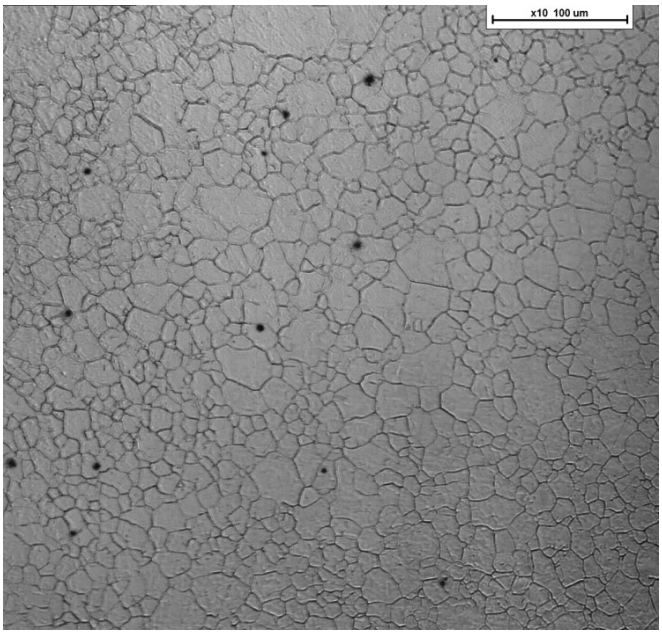

Fig. 17: Sample from Experiment 2 heated up to 1050°C.

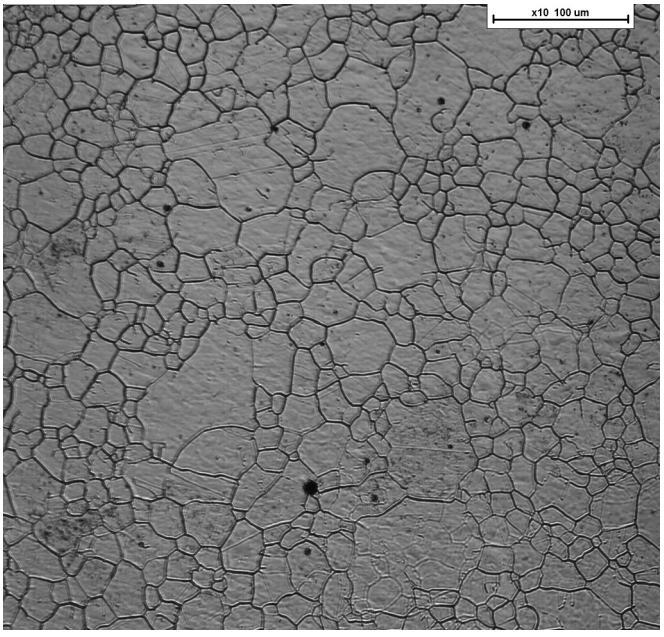

Fig. 18: Sample from Experiment 1 heated up to 1150°C.

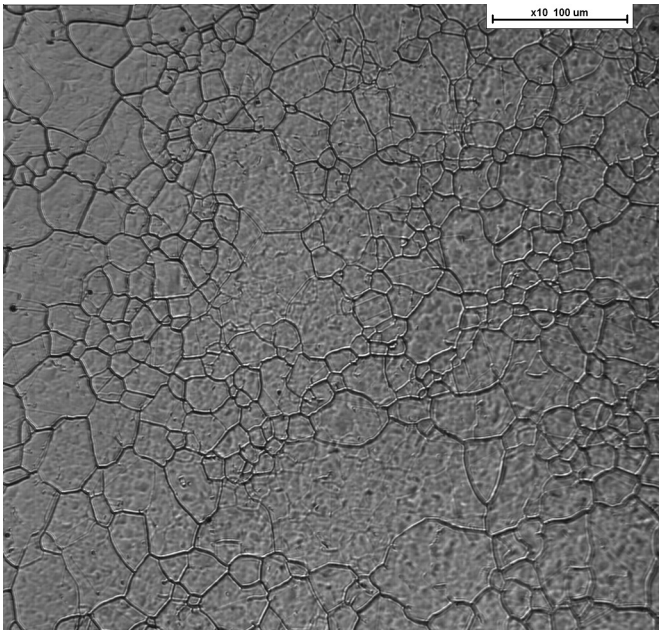

Fig. 19: Sample from Experiment 2 heated up to 1150°C.

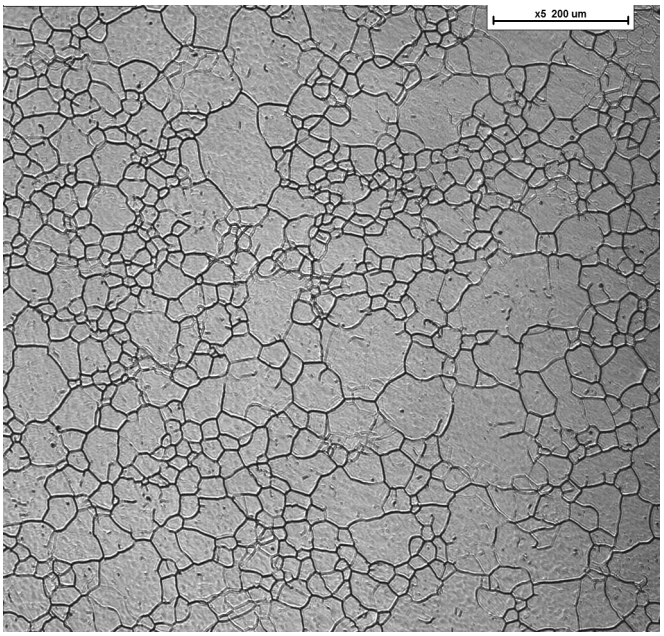

Fig. 20: Sample from Experiment 1 heated up to 1250°C.

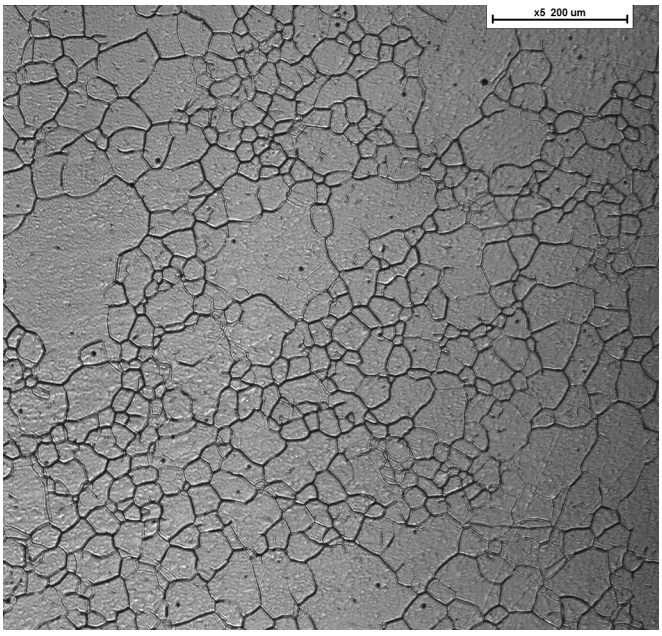

Fig. 21: Sample from Experiment 2 heated up to 1250°C.

3.1.2 Dual-stage heating

As it can be seen in Fig. 22, the dual stage heating treatment consisted of two different heating intervals and holding temperatures (950°C, and 1250°C).

The sample was heated first at a rate of 10 Ks^{-1} to a soak temperature of 950°C. This temperature was hold for 90 s. Subsequently a second heating stage took place, where the sample was heated at a rate of 1 Ks^{-1} to a soak temperature of 1250°C. Here the temperature was held for a short time before cooling down. Pictures were taken in situ during the whole length of the experiment at a rate of 10 frames per second.

Two micrographs were analyzed after having reached the two holding temperatures. Average grain size and grain size distribution were evaluated for the two selected micrographs, triangles in Fig. 22.

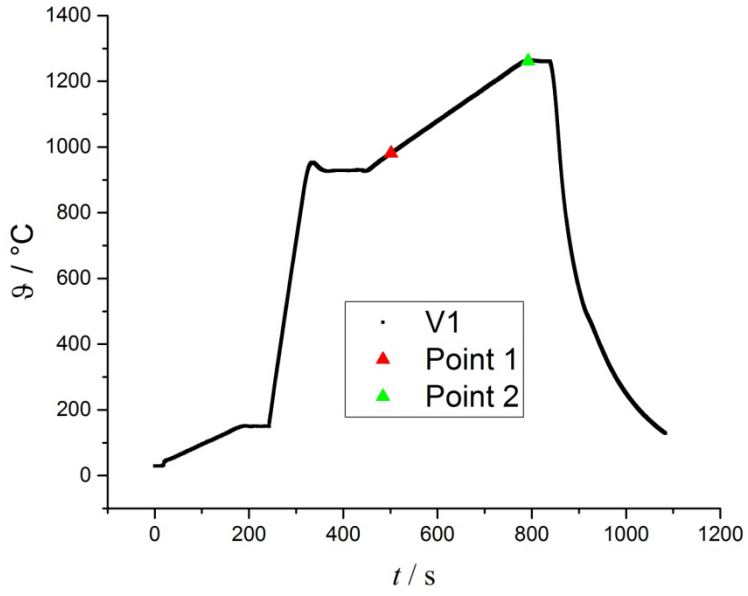

Fig. 22: Dual stage heating temperature profile with 2 points of investigation.

3.2 LUT experimental procedure

The experiments were accomplished in “The Centre for Metallurgical Process Engineering”, at the University of British Columbia (UBC). Procedure and results can be followed in [3].

Specimens were polished and etched using conventional metallographic techniques. The surfaces in the measurement area have a smooth finish to minimize the effect of surface roughness on ultrasound attenuation. [3]

The tests were performed under an Argon atmosphere to avoid oxidation. The specimens were heated at a rate of 10 Ks^{-1} to various soak temperatures (i.e. 1050°C 1150°C and 1250°C) After holding for about 15 to 20 min the samples were naturally cooled. [3]

The obtained numbers for average grain size were calibrated to be area-weighted values and are in this way able to compare with HT-LSCM obtained results.

4 Experimental Results

In this section, the results of the HT LSCM and LUT experiments will be illustrated. The results of the isothermal holding experiments for both techniques (i.e. HT LSCM and LUT) will then be compared in chapter 5.3.

4.1 HT LSCM results

In this section, the results from two different heating profiles will be discussed.

The heating profiles were already shown in Fig. 9 (Isothermal holding) and Fig. 22 (Dual-stage heating).

4.1.1 Grain growth during isothermal holding

In the videos, it is possible to observe austenite grain-size evolution throughout the whole length of the heating phase and for a time, once the soak temperature is reached. The visibility of the grain boundaries increases with time once the soak temperature is reached. At a certain point in time, the grain boundaries will be clear enough for grain size evaluation.

The grain structure firstly becomes visible after time t_1. The mean grain size at t_1 was determined for the sample heated up to a soak temperature of 1150°C (Fig. 12). No further grain growth has been observed after times t_2. The final average grain size (i.e. the grain size at t_2) has been obtained from the micrographs shown in Fig. 11, Fig. 13 and Fig. 15, respectively. It can be clearly seen that the average grain size increases with increasing soak temperatures.

Following the ASTM international standards for determining average grain size, the samples were investigated using the linear intercept method in each recording field [27] [28]. To accomplish the statistical requirements of at least 250 grains to be cut, a proper magnification was used.

The number of intersections in the recording field was evaluated with Linecut, a GUI of Matlab [29]. The average grain size of the X80 steel austenite grains was determined by calculating the mean value:

$\langle X \rangle = \frac{\sum X_i}{n}$, where X_i represents an individual value, $\langle X \rangle$ is the mean value and n is the number of measurements.

A sample temperature of 900°C was taken as time-zero t = 0 s [3]. Starting from this point in time, the best images were taken for grain size measurements.

In Experiment 1, it was possible to evaluate the grain size distribution only in micrographs with already developed structure, i.e. at final conditions t_2.

Table 5: Average grain diameters for different soak temperatures at different times for Experiment 1.

	Conditions to t_1			Conditions to t_2		
Sample	t [s]	n° of grains	d [µm]	t [s]	n° of grains	d [µm]
1050°C	---	---	---	241.1	293	19.6
1150°C	---	---	---	240.2	217	26.8
1250°C	---	---	---	252.2	240	49.3

In Experiment 2, it was possible to make grain size evaluations at earlier times t_1. However, only one micrograph satisfied the evaluation requirements, while the others are subjected to many assumptions, and are therefore only approximate results that can be taken only as a reference.

Table 6: Average grain diameters for different soak temperatures at different times for Experiment 2.

	Conditions to t_1			Conditions to t_2		
Sample	t_1 [s]	number of grains	d [µm]	t_2 [s]	number of grains	d [µm]
1050°C	180.07	406	14.4	242.78	337	17.4
1150°C	94.84	267	21.6	257.28	189	30.1
1250°C	66.23	363	15.8	270.91	218	53.1

4.1.1.1 Grain size distribution of the samples heated to 1050°C

The histograms for the grain size distribution are shown in Fig. 24 (1050°C), Fig. 28 (1150°C) and Fig. 34 (1250°C) for Experiment 1 and in Fig. 26 (1050°C), Fig. 30 and Fig. 32 (1150°C) and Fig. 36 (1250°C) for Experiment 2.

Experiment 1

The mean grain size d_2 at t_2 = 241.08 s was d_2 = 19.6 µm.

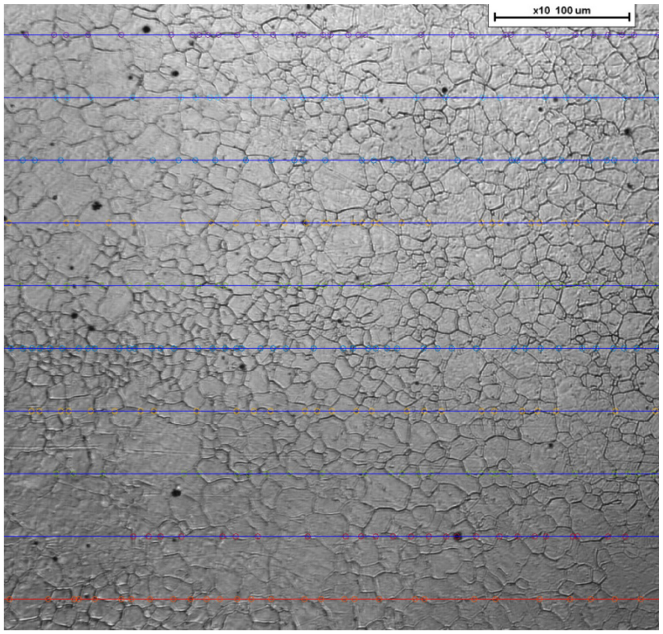

Fig. 23: Evaluation of grain size distribution at t_2 (1050°C).

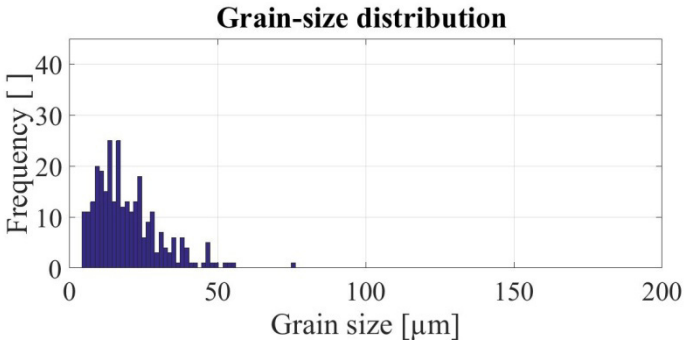

Fig. 24: 50 sections histogram at t_2 = 241.08 s (1050°C).

Experiment 2

The mean grain size d_2 at t_2 = 242.78 s was d_2 = 17.4 µm.

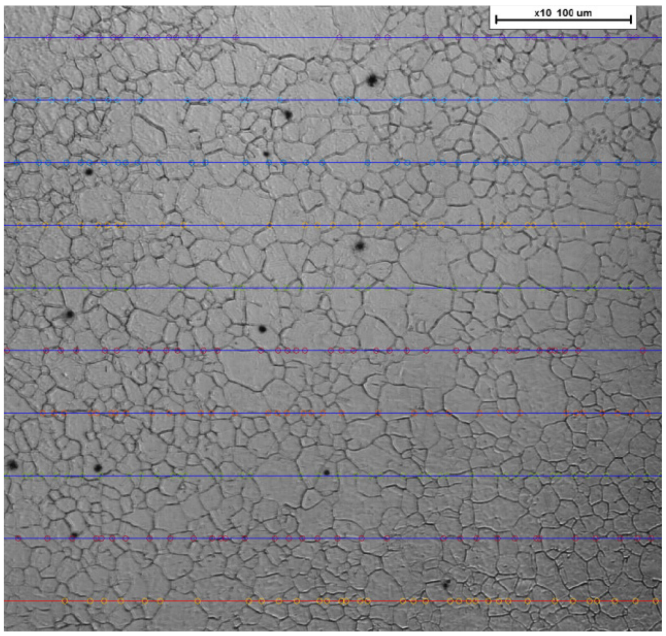

Fig. 25: Evaluation of grain size distribution at t_2 (1050°C).

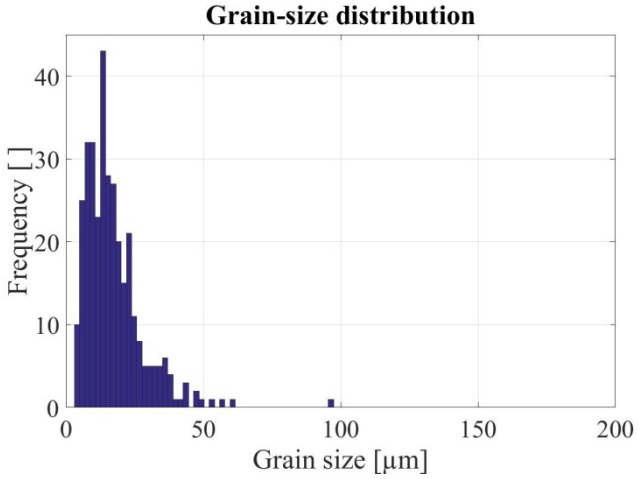

Fig. 26: 50 sections histogram at t_2 = 242.78 s (1050°C).

4.1.1.2 Grain size distribution of the samples heated to 1150°C

At this soak temperature, it was possible to evaluate the grain size distribution in Experiment 2 two times. One of the evaluations was carried out shortly after having reached the soak temperature with clearly visible grain boundaries, yellow square in Fig. 37. The second evaluation was carried out once the microstructure became stable and did not change anymore in time, yellow circle in Fig. 37.

In Experiment 1, evaluation was possible only after having reached final conditions. Time and temperature values of Experiment 1 (yellow star in Fig. 37) lay in-between the values gained for the different time-temperature couples in Experiment 2.

Experiment 1

The mean grain size d_2 at t_2 = 240.2s was d_2 = 26.8 µm.

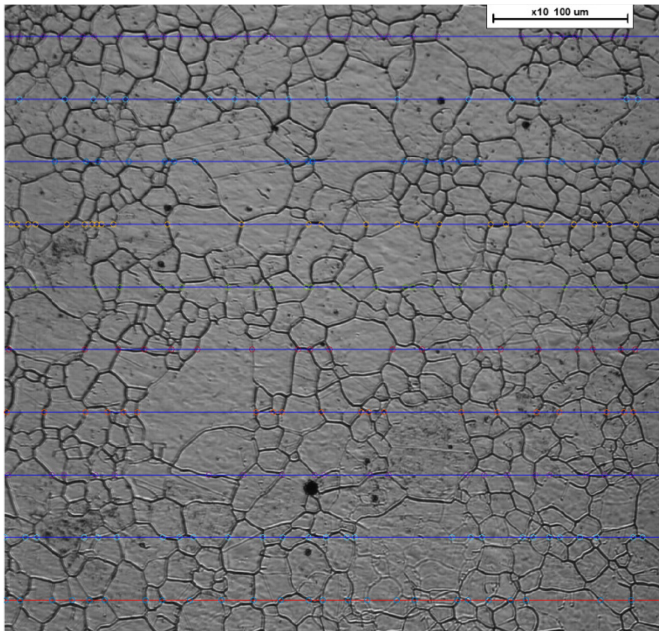

Fig. 27: Evaluation of grain size distribution at t_2 (1150°C).

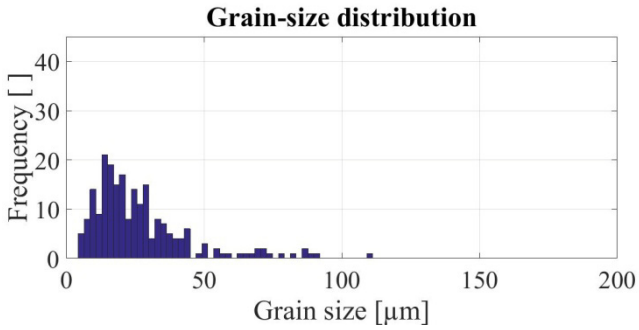

Fig. 28: 50 sections histogram at t_2 = 240.2 s (1150°C).

Experiment 2

The mean grain size d_1 at t_1 = 94.841 s was d_1 = 21.6 µm. The mean grain size d_2 at t_2 = 257.3 s was d_2 = 30.1 µm.

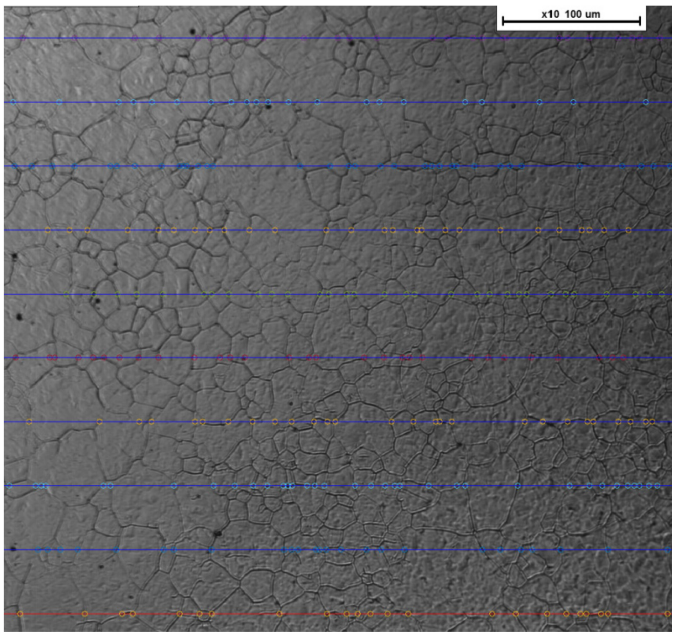

Fig. 29: Evaluation of grain size distribution at t_1 (1150°C).

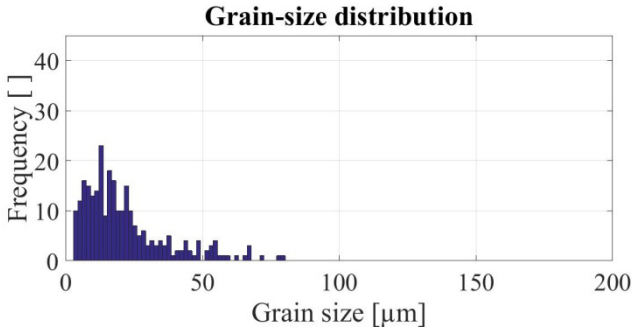

Fig. 30: 50 sections histogram at t_1= 94.84 s (1150°C).

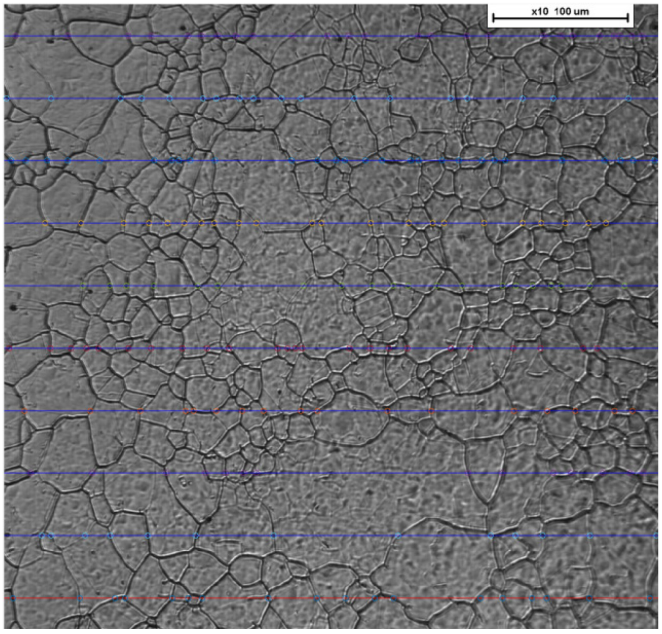

Fig. 31: Evaluation of grain size distribution at t_2 (1150°C).

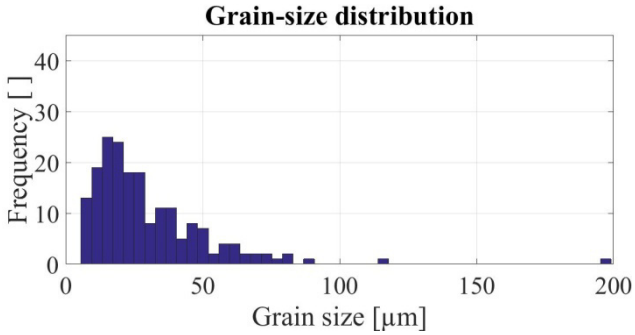

Fig. 32: 50 sections histogram at t_2 = 257.28 s (1150°C).

4.1.1.3 Grain size distribution of the samples heated to 1250°C

Experiment 1

The mean grain size d_2 at t_2 = 252.2 s was d_2 = 49.3 µm.

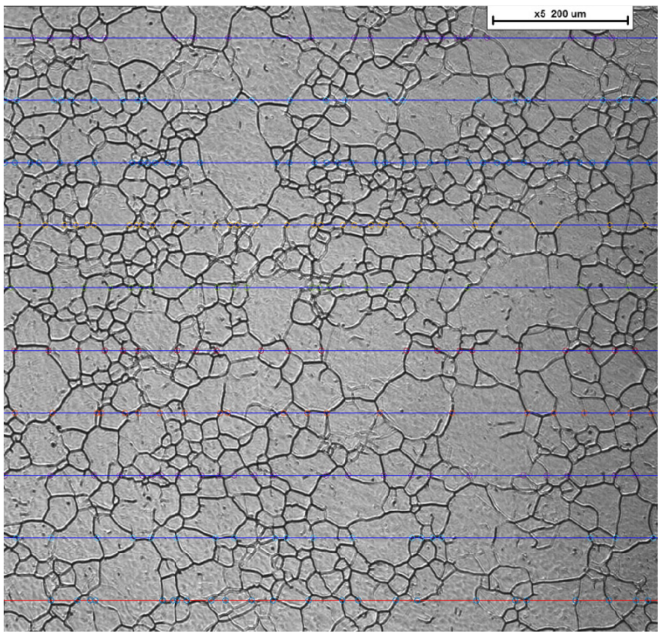

Fig. 33: Evaluation of grain size distribution at t_2 (1250°C).

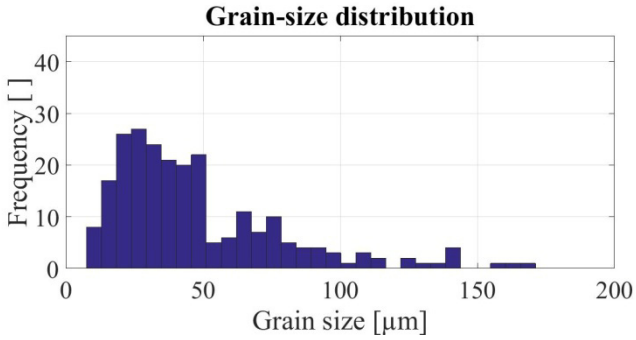

Fig. 34: 50 sections histogram at t_2 = 252.2 s (1250°C).

Experiment 2

The mean grain size d_2 at t_2 = 270.91 s was d_2 = 53.1 µm.

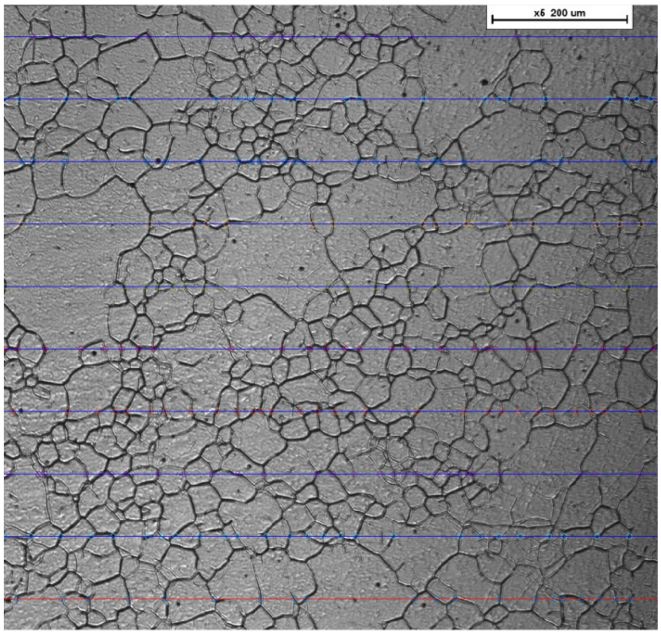

Fig. 35: Evaluation of grain size distribution at t_2 (1250°C).

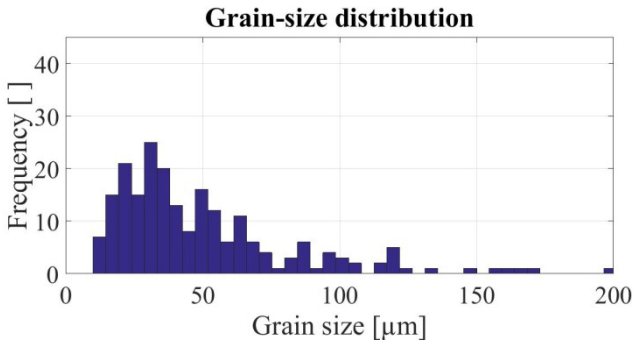

Fig. 36: 50 sections histogram at t_2 = 270.91 s (1250°C).

The grains at 1250°C (Fig. 14 and Fig. 15) are much larger than the grains for the other two soak temperatures 1050°C (Fig. 10 and Fig. 11) and 1150°C (Fig. 12 and Fig. 13) at any time. Therefore, due to the already discussed statistical requirements, a different magnification had to be used for the evaluation of the samples heated up to 1250°C (Fig. 33 and Fig. 35). A magnification of half of the magnification used for the other two soak temperatures was used for grain size evaluation at a soak temperature of 1250°C.

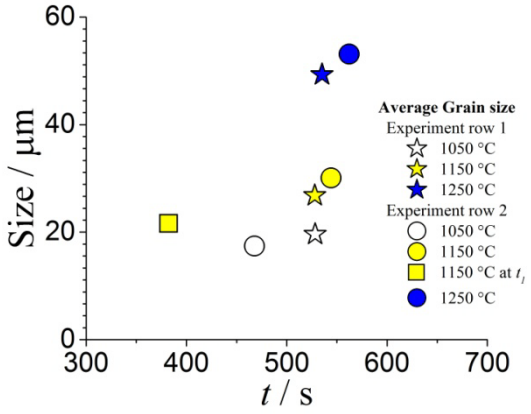

Fig. 37: Summary of gained average grain sizes for the isothermal holding experiments.

4.1.2 Grain growth during dual-stage heating

A sample temperature of 900°C was taken as time-zero t = 0 s for this experiment as well [3].

The mean grain size after 187.4 s was 11.44 µm. This is, after the first soak temperature was reached.

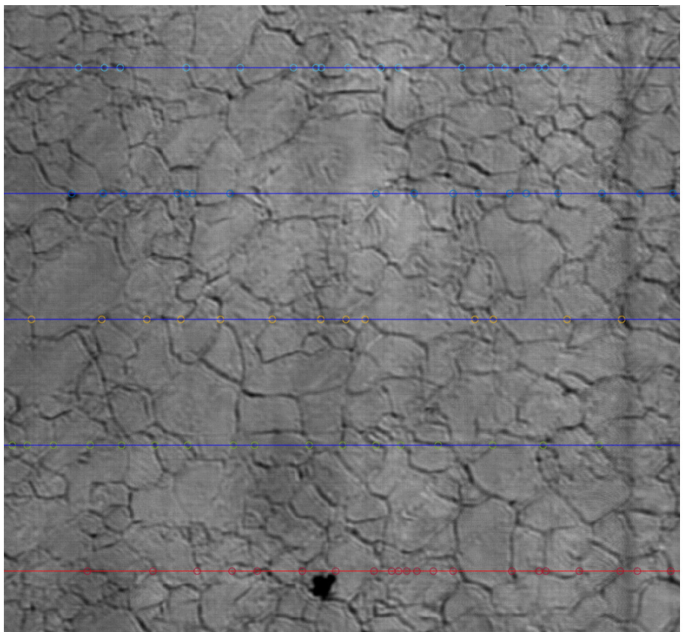

Fig. 38: Evaluation of grain size distribution (1005.5°C).

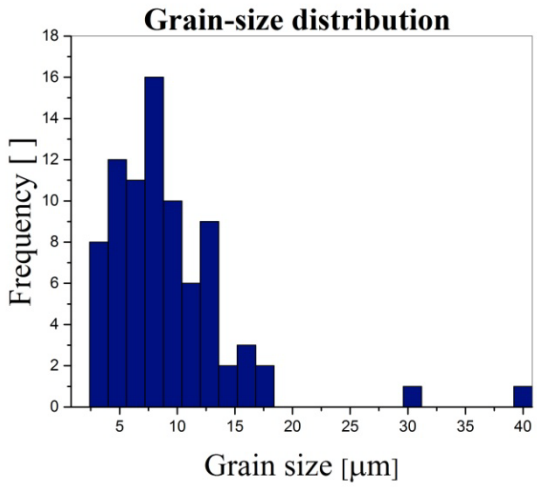

Fig. 39: 25 sections histogram after 187.4 s (1005.5°C).

The mean grain size after 478.3 s was 31.76 µm. This is, after the second soak temperature was reached.

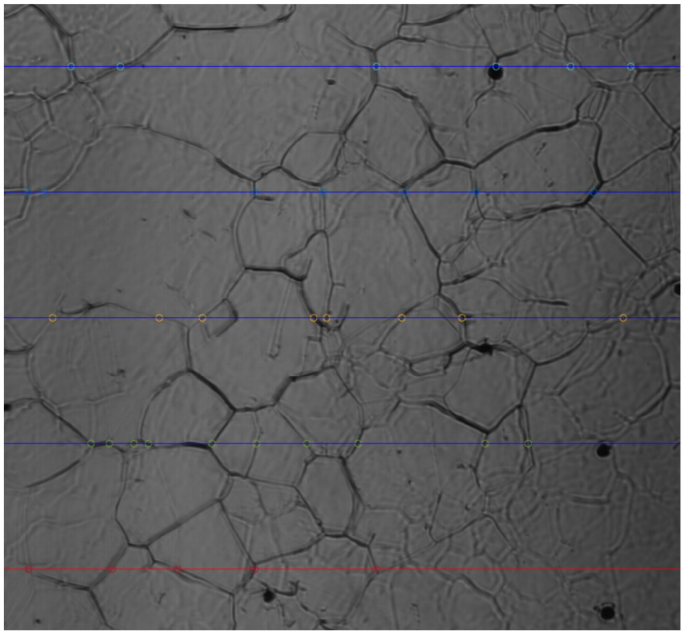

Fig. 40: Evaluation of grain size distribution (1251.2°C).

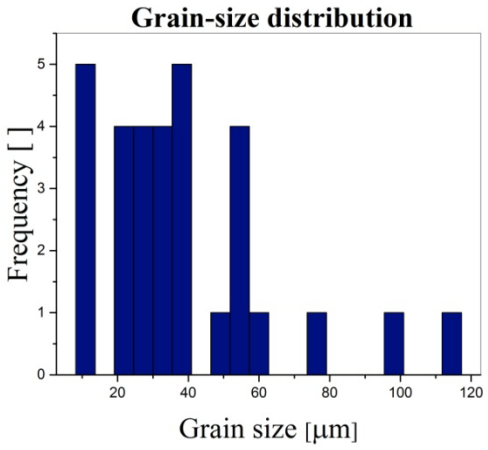

Fig. 41: 25 sections histogram after 478.3 s (1251.2°C).

4.2 LUT results

Fig. 42 shows the results gained at The Centre for Metallurgical Process Engineering in [3], when measuring austenite grain-growth behavior by LUT at 10 Ks^{-1} heating rate followed by various isothermal holding temperatures. The curves reach a plateau (see dashed lines in Fig. 42) indicating that a grain size was reached for each soak temperature [3]. Although the LUT is a volumetric method, the results were converted to area-weighted values in order to compare them with other metallographic measurements.

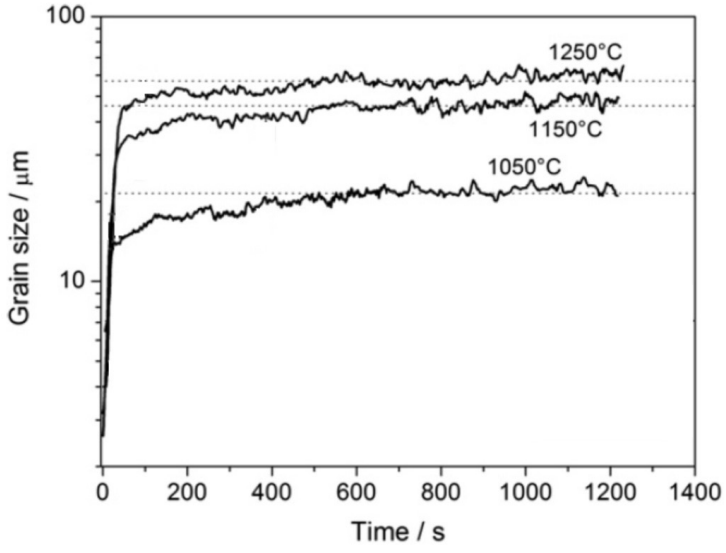

Fig. 42: Resulting LUT average area weighted grain sizes over time. Time zero corresponds to 900°C

5 Discussion

In this section, the grain size distribution of the samples from Experiment 2 of the isothermal holding experiments will be evaluated using a number density function and an area density function.

The kinetics of grain growth will be briefly discussed by showing, how triple points move during heat treatment.

Finally, the measured average grain-size values of the two methods (HT LSCM and LUT) will be compared.

5.1 Grain-size distribution

By a careful interpretation of the micrographs from Fig. 25, Fig. 29, Fig. 31, and Fig. 35, the multimodal nature of the grain size distribution can be observed.

Many small grains and some medium ones are present in Fig. 25, implying a bimodal distribution. In Fig. 29 and Fig. 31, a lot of small grains, many medium-sized grains and some large-sized grains are present. This implies the existence of a trimodal distribution. Finally, in Fig. 35 there are many grains in different size ranges, leading to a multimodal distribution.

When evaluating the images with the number fraction distribution, i.e. measuring the frequency of the grains given in a selected grain diameter range, this multimodal grain size distribution disappears, as it can be seen in Fig. 43, Fig. 45, Fig. 47, and Fig. 49. In the case of an evenly distribution of small and big grains (i.e. of the total area 50% are small and the rest big), in a given area there will be always present many more small grains than big grains. Therefore, it is necessary to find another means of weighting the grain size distribution. This could be achieved by an area-weighted approach as it was proposed by Laszlo S. Toth in [30].

As it can be observed from Fig. 44, Fig. 46, Fig. 48, and Fig. 50, the evaluation of the grain size distribution using the area-weighted approach reassembles better reality. With reality is meant the first impression that is gained when the reader looks at the micrographs with the naked eye as it has been just now discussed. The area-weighted grain-size distribution approach consists on measuring the area, which grains in a certain diameter range constitute.

An, approximately, log normal distribution but with an extra peak at the end of the distribution can be seen in Fig. 44, leading in this way to a bimodal distribution, where small grains prevail over bigger ones. A rather normal distribution with two additional peaks can be seen in Fig. 48 leading in this way to a trimodal distribution. In Fig. 50 it can be seen a distribution that would be given for a multimodal distribution.

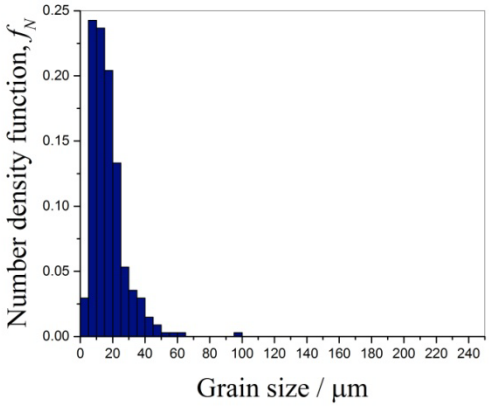

Fig. 43: Number weighted grain size distribution for 1050°C soak temperature at t_2.

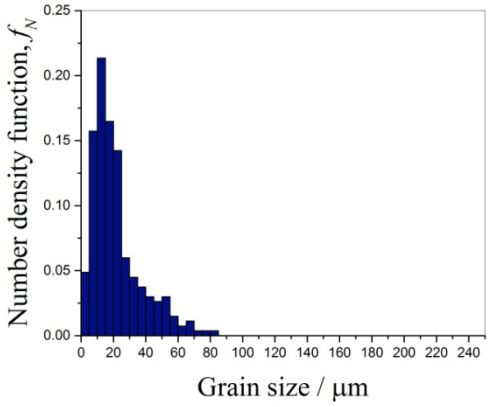

Fig. 45: Number weighted grain size distribution for 1150°C soak temperature at t_1.

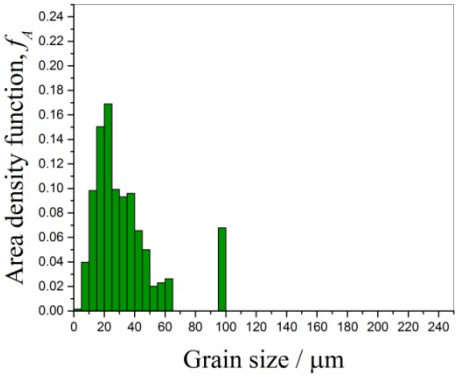

Fig. 44: Area weighted grain size distribution for 1050°C soak temperature at t_2.

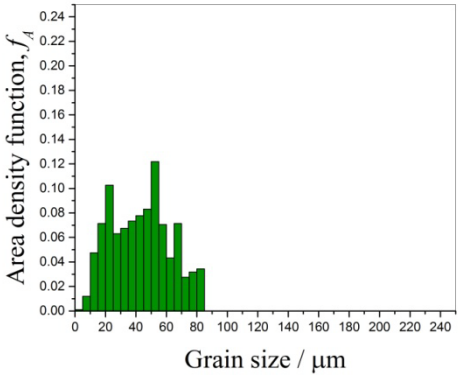

Fig. 46: Area weighted grain size distribution for 1150°C soak temperature at t_1.

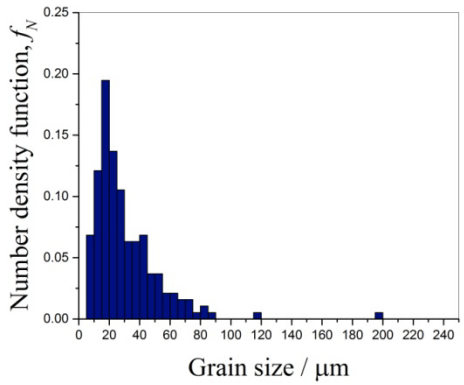

Fig. 47: Number weighted grain size distribution for 1150°C soak temperature at t_2.

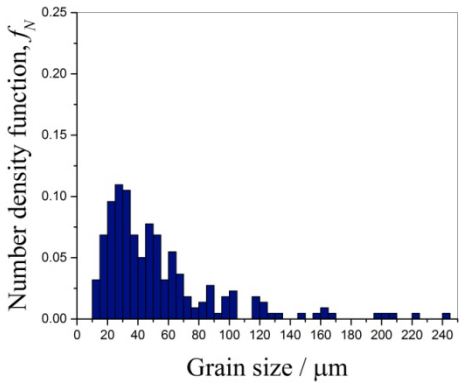

Fig. 49: Number weighted grain size distribution for 1250°C soak temperature at t_2.

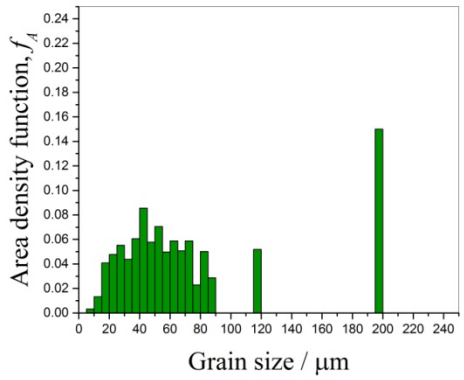

Fig. 48: Area weighted grain size distribution for 1150°C soak temperature at t_2.

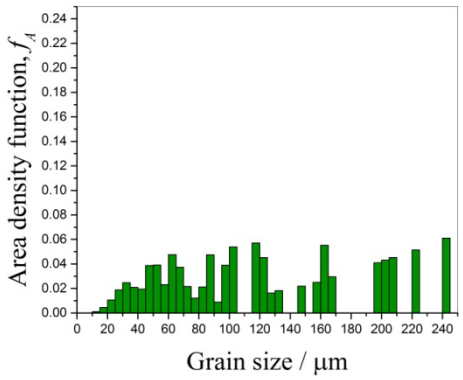

Fig. 50: Area weighted grain size distribution for 1250°C soak temperature at t_2.

In this way, it was shown that the area density function approach is a better one than the number density function approach at the moment of evaluating the grain size distribution. It has been shown that the number density function hides the multimodal nature of the distribution if given, whereas the area density function highlights the existence of such a distribution.

Since it has been shown that the distribution of the grain size plays a role as important as the average grain size plays in the material properties [17], it is of crucial importance to use an area or volume weighted approach for evaluation of the grain size distribution.

From comparing Fig. 44, Fig. 48, and Fig. 50, it can be seen that the grain size distribution becomes more multimodal with increasing soak temperature. The way in which grain boundaries move, changing thus the average grain size and the grain size distribution is

subject of the kinetics of grain growth. Subsequent the movement of triple points of grain boundaries will be discussed.

5.2 Movement of triple points in grain growth

The in-situ evolution of the grain sizes can be observed in some regions of the sample surface by investigating the motion of the migrating grain boundaries. This is possible by watching the movies in an appropriate play / play-back speed. Details concerning the growth process in these regions can be visualized by depicting grain structures at earlier and later stages.

For the measurement of the velocity at the grain boundary, the movement of triple junctions was analysed (Fig. 51). The first moment at which the triple junction was recognizable, was chosen as the initial condition t = 0 s (Table 7). Thus for different triple junctions different times were selected as t = 0 s. A point in time, when significant displacement of the triple junction did not take place anymore, was selected as the final condition. The time difference between final and initial conditions divided by the number of steps -1 gives the space of time between the evaluation steps.

$$t_{step} = \frac{t_{final} - t_{initial}}{n-1}$$

t_{step} … Time interval between evaluation steps

t_{final} … Time at final conditions, i.e. the point in time at which the triple junction does not change position significantly anymore.

$t_{initial}$ ... Time at initial conditions, i.e. the point in time at which the triple junction is recognizable.

n … Number of evaluation steps.

After having plotted the triple points at all time-steps, these plots were placed together in one plot, Fig. 51. In this manner, it was possible to determine the movement of the triple points as time passed by and consequently their velocity.

Evaluation was done than every 4.24 s until the movement of the triple junction was insignificant.

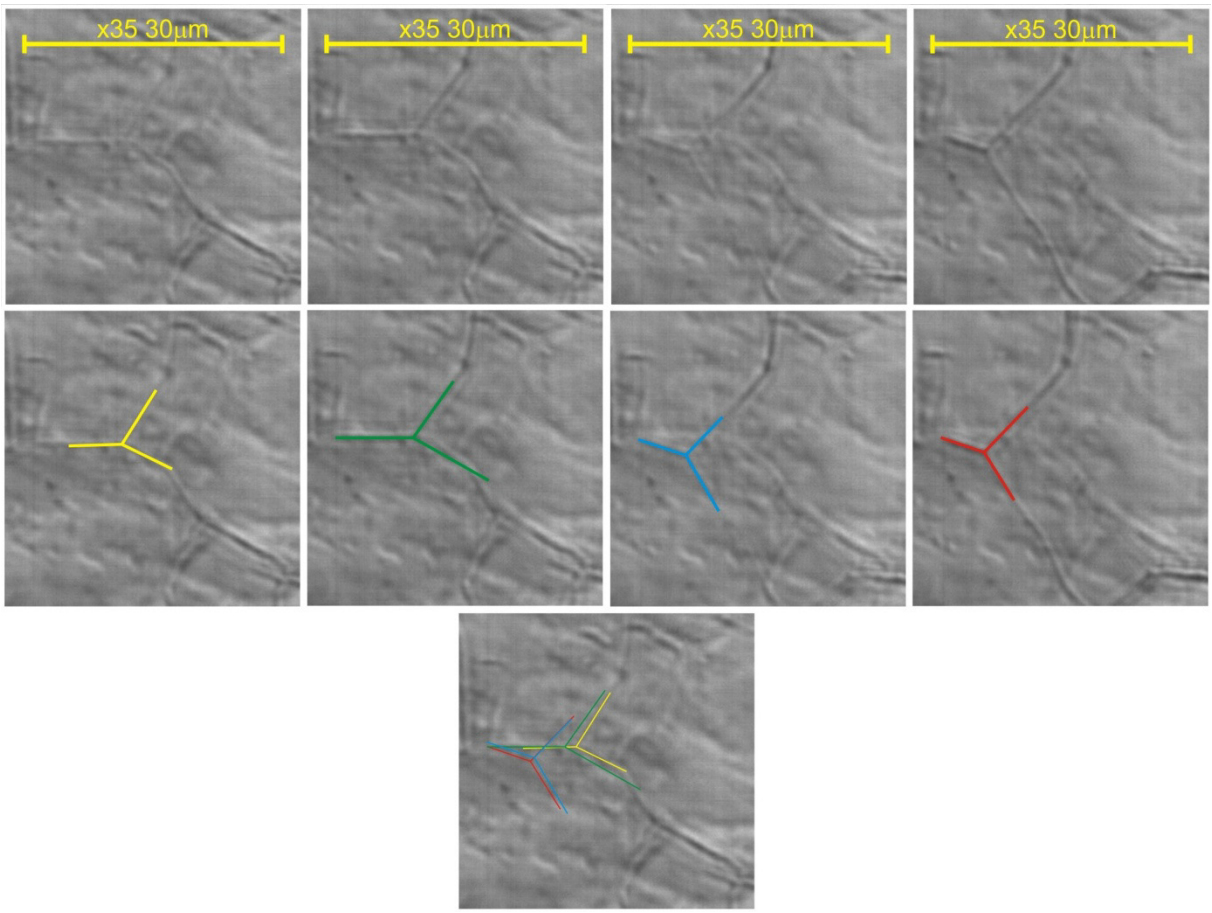

Fig. 51: Motion of triple junctions.

From the summary picture of Fig. 51, it is possible to recognize that grain boundaries have no constant velocity. Given that time steps are constant, it is possible to deduce from Fig. 51 that the velocity at the beginning is very low and that a phase of great displacement, i.e. high velocity follows. Finally, once more, a period of very small velocity occurred until the boundary remained stationary.

Table 7: Average grain diameters for different soak temperatures at different times.

Time [s]	Time steps[s]	Temperature [°C]
328.84	0	1159.9
333.08	4.24	1159.5
337.32	8.48	1158.4
341.56	12.72	1156.4

At elevated temperatures, grain boundaries want to move in direction of the radius of curvature, so letting grow some grains at expenses of others, as seen in chapter “2.2 Grain Growth”. In this case, it is being dealt with microalloyed steels with Niobium carbide in its structure. Niobium carbides are frequent intentional products in microalloyed steels due to its extremely low solubility in austenite and its ability to prevent excessive grain growth [31].

From Fig. 51 it is assumed that grain boundaries move freely at low velocities until they are trapped by Niobium carbides. From this point on, forces build up in this grain boundary. A point is going to be reached, at which the forces are too big for the Niobium carbides to still restrain grain boundary movement, so that a dissolution process will take place presumably. Due to the force being released, the boundary is submitted at the beginning to a very high acceleration. Correspondingly, a high velocity will be expected until the boundary is once more trapped by the next Nb carbides. All of these steps can be followed in Fig. 51.

5.3 LUT & HT-LSCM comparison

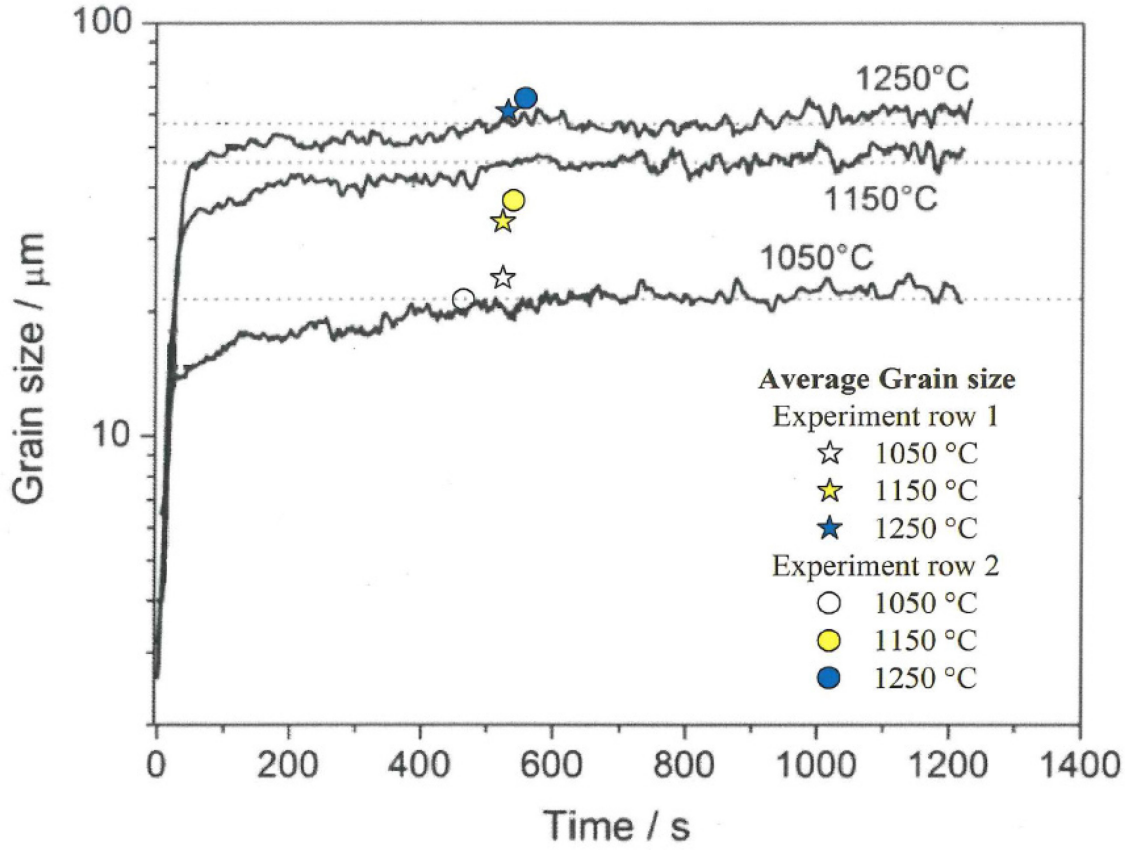

Fig. 52: Comparison between average area-weighted LUT and HT-LSCM grain size measurements.

The data provided by The Centre for Metallurgical Process Engineering in [3] shows an average value for grain-size at different points in time. LUT measurements do not provide any information about grain-size distribution. For example, in an extreme case, it could be that a bimodal grain size distribution exists. This could consist of many small grains and some very large ones. Clearly, such a grain-size distribution would account for very bad material-properties. By means of LUT, only the averaged grain size would be provided and therefore better material properties than the given ones would be predicted.

Although by means of LUT very accurate average grain-sizes can be provided, in some cases it will require the assistance of another in-situ measurement technique. Especially

when bimodal or multimodal grain-size distributions are expected, the analysis of the grain-size distribution is essential. Notwithstanding that HT-LSCM is a surface technique, its evaluation provides not only with the average grain-size but it supplies with information about the grain-size distribution as well.

By using the HT-LSCM and the linear intercept method for determination of average grain size and grain size distribution, a linear weighted average grain size will be determined. In contrast, by means of LUT a volume weighted average grain size can be provided. Comparison of these measured average grain sizes would not make any sense at all. Since the given LUT data was already converted to area weighted average grain sizes in [3], the data gained with HT-LSCM must be converted to area-weighted values as well.

Grain size measurements are usually performed in planar sections. Therefore, procedures were developed to estimate three dimensional grain sizes from two-dimensional measurements [17]. At the moment of converting 2D measured grain sizes to 3D grain sizes and vice versa, certain effects must be taken into account. E.g. the truncation effect (probability that the planar section reveals a diameter that is less than the actual diameter of the grain) and the sampling effect (it is more likely that a large grain will be intersected by a plane than a small grain) [17].

In [17] a conversion factor was derived in order to transform measured linear weighted average grain sizes to area and volume weighted average grain sizes. Takayama et al. assumed that grains have a tetrakaidecahedral shape, thereby allowing for space filling. This approach draws on the fact that random lines that intercept a given volume will produce a probability distribution, which relates the intersection length with the equivalent volume diameter. A lognormal grain size distribution will be given and the average grain size will be gained from this distribution [17].

Takayama et al. reported the mean linear intercept length l_m, and the mean grain area A_m to be functions of the standard deviation s_V of the three-dimensional grain size distribution and the grain size d_{Vm} [17].

$$l_m = 0.60661 \cdot d_{Vm} \cdot \exp(2.5 \cdot (\ln s_V)^2)$$
$$A_m = 0.4861 \cdot {d_{Vm}}^2 \cdot \exp(4 \cdot (\ln s_V)^2)$$

During normal grain growth, the distribution width will not change significantly and the mean grain size will increase steadily. In this manner, an average value for the standard deviation can be used during normal grain growth. For the grain size distributions discussed in this thesis, a standard deviation of 1.33 will be used, as recommended in [17]. By inserting this value in above formulas, following is obtained:

$$A_m = 0.4861 \cdot {d_{Vm}}^2 \cdot \exp(4 \cdot (\ln 1.33)^2) \quad \rightarrow \quad A_m = 0.6729 \cdot {d_{Vm}}^2 \quad \rightarrow \quad d_{Vm} = 1.22 \cdot A_m$$

It is concluded that the mean equivalent volume diameter d_{Vm} is approximately 20% greater than the mean equivalent area diameter A_m. In addition, a comparison done in [17] reveals that d_{Vm} is 50% greater than l_m, being in this way able to write the approximate general equation:

$$d_{Vm} = 1.2 d_{Am} = 1.5 l_m .$$

For a comparison of both methods (LUT and HT-LSCM) to take place, the linear weighted results from HT LSCM were transformed to area-weighted values after [17]:

$$1.2 d_{Am} = 1.5 l_m \rightarrow d_{Am} = \frac{1.5}{1.2} l_m \rightarrow d_{Am} = 1.25 l_m$$

A comparison of both techniques is reasonable as long as abnormal grain growth did not take place.

It must be taken into account that with increasing soak temperature the width of the grain size distribution will increase as well, because of abnormal grain growth taking place, as it can be seen from Fig. 46, Fig. 48, and Fig. 50. It can be expected that a temperature will be reached, at which the grain size distribution after the number density function will not show any more a log normal distribution and a conversion from linear to volume-weighted values after Takayama [17] is not going to be possible or will deliver wrong values.

As it can be seen in Fig. 52, the measured average grain sizes of both techniques match reasonable well. The maximum deviation is lower than 30%. The heat treatment with a soak temperature of 1150°C shows the biggest error between the LUT and HT-LSCM resulting average grain sizes. The average grain sizes gained by LUT and HT-LSCM in the other heat treatments show almost no error.

6 Conclusion/ Interpretation/ Recommendations

An accurate evaluation of grain sizes during the heating time was not possible using the HT-LSCM in the investigated heat treatments. Once the soak temperature is reached, the grain-boundaries became clearer with time and grain growth could be observed as well as grain sizes could be accurately measured. As expected the final average grain size is larger for higher soak temperatures.

The distribution of the grains in the investigated steel is not uniform but rather a multimodal-distribution of grain sizes was observed. Nevertheless when evaluating the micrographs with the number fraction distribution, i.e. measuring the frequency of the grains given in a selected grain diameter range, this multi-modal grain size distribution disappears. An evaluation with the area-density-function, i.e. measuring the area that grains given in a selected grain diameter range constitute, highlights the multi-modal nature of the grain size distribution, if given.

As it can be seen from comparing Fig. 43 and Fig. 44, or Fig. 45 and Fig. 46, or Fig. 47 and Fig. 48, or Fig. 49 and Fig. 50, by means of the number-density-function, material properties would be misinterpreted. They would be accounted as better than the predicted by the area-density-function evaluation.

The analysis of the motion of triple points resulted in Fig. 51. This shows that the velocity of the grain boundaries is not constant. After motion of the grain boundary has started, the forces that built up on the grain boundary subject it to a great acceleration and the grain boundary will move fast for a given period of time. Afterwards that the grain boundary suffers a negative acceleration, probably because of it being trapped by the next NbC. In this way, the velocity of the grain boundary is very low before stopping.

For further investigation of kinetics of grain growth, I recommend not to look just for an average velocity. Velocity profiles from the beginning to the end of motion of the grain boundary should be obtained from different grains and compared. A comparison of many different velocity profiles could be carried out in order to gain meaningful insight in the understanding of kinetics of grain growth.

Comparison of the resulting average grain-size measurements of both techniques, i.e. LUT and HT-LSCM, match reasonable well, confirming that both techniques complement each other in certain cases. Despite the drawbacks of both techniques, better prediction of the material properties using both techniques is possible, because their strengths are different and make up for the drawbacks of the other technique.

The HT LSCM technique provides not only with the average-grain-size values but with the grain size distribution as well. The main disadvantage of the HT LSCM technique is being a surface technique. As the soak temperature increases, some grains will be energetically favoured to grow more rapidly than others do. When this takes place at a large scale, abnormal grain growth is taking place and the grain size distribution is going to change, becoming more and more multimodal, as it can be seen from comparing Fig. 44, Fig. 48, and Fig. 50. A conversion of linear values to surface values, with the method that has been discussed here, cannot be applied if abnormal grain growth is taking place.

Although the accuracy of average grain size measurements with LUT is higher as well as its resolution (i.e. number of average grain size measurements over time), as compared with the HT LSCM technique, it does not provide any information about the grain size distribution, which may be of crucial importance for the prediction of material properties.

Since the grain size distribution is as important as the average grain size for the determination of material properties, the HT LSCM technique is required when the grain size distribution is unknown or when a multimodal distribution is expected.

References

[1] K. Banerjee, M. Militzer, M. Perez and X. Wang, “Nonisothermal Austenite Grain Growth Kinetics in a Microalloyed X80 Linepipe Steel,” *Metallurgical and Materials Transactions A,* no. 41A, pp. 3161-3172, 2010.

[2] P. Schaffnit, C. Stallybrass, J. Konrad, A. Kulgemeyer and H. Meuser, “Dual-scale phase field simulation of grain growth upon reheating of a microalloyed line pipe steel,” *International Journal of Materials Research,* no. 101, pp. 549-554, 2010.

[3] M. Maalekian, R. Radis, M. Militzer, A. Moreau and W. J. Poole, “In situ measurement and modeling of austenite grain growth in a Ti/Nb microalloyed steel,” *Acta Materialia,* no. 60, pp. 1015-1026, 2012.

[4] The_World_Factbook, “Central Intelligence Agency,” [Online]. Available: https://www.cia.gov/library/publications/the-world-factbook/fields/2117.html.

[5] ILF Consulting Engineers Tim Callan, “Pipeline Technology Today and Tomorrow,” ÖGEW, DGMK Herbstveranstaltung 2007, 2007.

[6] Q. Sha and Z. Sun, “Grain growth behavior of coarse-grained austenite in a Nb-V-Ti microalloyed steel,” *Materials Science and Engineering A,* no. 523, pp. 77-84, 2009.

[7] M. Maalekian, “The Effects of Alloying Elements on Steels,” Technical report at the Christian Doppler Laboratory for Early Stages of Precipitation, Technische Universität Graz. Institut für Werkstoffkunde, Schweißtechnik und Formgebungsverfahren, 2007.

[8] L. Zheng, Z.-x. Yuan, S.-h. Song, T.-h. Xi and Q. Wang, “Austenite Grain Growth in Heat Affected Zone of Zr-Ti Bearing Microallozed Steel,” *Journal of iron and Steel Research, International,* no. 19, pp. 73-78, 2012.

[9] Y. Gu, P. Tian, X. Wang, X.-l. Han, B. Liao and F.-r. Xiao, “Non-isothermal prior austenite grain growth of a high-Nb X100 pipeline steel during a simulated welding heat cycle process,” *Materials and Design,* no. 89, pp. 589-596, 2016.

[10] J. Fernández, S. Illescas and J. M. Guilemany, “Effect of microalloying elements on the austenitic grain growth in a low carbon HSLA steel,” *Materials letters,* no. 61, pp. 2389-2392, 2007.

[11] T. Garcin, J. H. Schmitt and M. Militzer, “In-situ laser ultrasonic grain size measurement in superalloy,” *Journal of Alloys and Compounds.,* no. 670, pp. 329-336, 2016.

[12] F. Z. Bu, X. M. Wang, L. Chen, S. W. Yang, C. J. Shang and R. D. K. Misra, “Influence of cooling rate on the precipitation behavior in Ti-Nb-Mo microalloyed steels during continuous cooling and relationship to strength,” *Materials Characterization,* no. 102, pp. 146-155, 2015.

[13] F. Z. Bu, X. M. Wang, S. W. Yang, C. J. Shang and R. D. K. Misra, “Contribution of intherphase precipitation on yield strength in thermomechanically simulated Ti-Nb and Ti-Nb-Mo microalloyed steels,” *Materials Science and Engineering A,* no. 620, pp. 22-29, 2015.

[14] M. Militzer, A. Giumelli, E. B. Hawbolt and T. R. Meadowcroft, “Austenite and Ferrite Grain Size Evolution in Plain Carbon Steels,” [Online]. Available: https://www.osti.gov/scitech/servlets/purl/10110118. [Accessed 11 09 2017].

[15] F. D. Fischer, J. Svoboda and K. Hackl, “Modelling the kinetics of a triple junction,” *Acta Materialia,* no. 60, pp. 4704-4711, 2012.

[16] M. Hillert, “On the theory of normal and abnormal grain growth,” *Acta Metallurgica,* no. 13, pp. 227-238, 1965.

[17] A. K. Giumelli, M. Militzer and E. B. Hawbolt, “Analysis of the Austenite Grain Size Distribution in Plain Carbon Steels,” no. 39, pp. 271-280, 24 11 1999.

[18] H. Azizi-Alizamini, M. Militzer and W. J. Poole, “A novel technique for developing bimodal grain size distributions in low carbon steels,” *Scripta Materialia,* no. 57, pp. 1065-1068, 2007.

[19] W. D. Callister and D. G. Rethwisch, Materialwissenschaften und Werkstofftechnik: Eine Einführung, Wiley-VCH Verlag GmbH & Co. KGaA, 2013.

[20] M. Oberndorfer, “Skriptum Metallurgie und Korrosion für Erdölingenieure,” Montanuniversität Leoben, 2015.

[21] “Wikipedia The Free Encyclopedia,” [Online]. Available: https://en.wikipedia.org/wiki/Carbon_steel. [Accessed 29 June 2017].

[22] D. A. Porter, K. E. Easterling and M. Y. Sherif, Phase Transformations in Metals and Alloys, Taylor & Francis Ltd, 2009 .

[23] “Computer Simulation Laboratory,” Middle East Technical University Metallurgical & Materials Engineering, 2005. [Online]. Available: http://www.csl.mete.metu.edu/gbgrooving/index.htm. [Accessed 11 09 2017].

[24] Bernhard Lässer ILF, “Skriptum Vorlesung Pipeline Engineering,” Montanuniversität Leoben, Lehrstuhl für Fördertechnik und Konstruktionslehre, 2009.

[25] SPE_International, “PetroWiki. Pipeline design consideration and standards,” [Online]. Available: http://petrowiki.org/Pipeline_design_consideration_and_standards. [Accessed 4 May 2017].

[26] N. Hülsdau, “Engineering new limits for large gas transportation systems,” *Journal for Piping, Engineering, Practice,* p. 6, 1 2006.

[27] ASTM, “Standard Test Methods for Determining Average Grain Size”. Patent E112.

[28] ASTM, “Standard Test Methods for Characterizing Duplex Grain Sizes”. Patent E1181.

[29] Matlab_R2015b_Academic_licence.

[30] L. S. Toth, S. Biswas, C. Gu and B. Beausir, “Notes on representing grain size distributions obtained by electron backscatter diffraction,” *Materials Characterization,* no. 84, pp. 67-71, 2013.

[31] “Wikipedia The Free Encyclopedia,” [Online]. Available: https://en.wikipedia.org/wiki/Niobium_carbide. [Accessed 24 Mai 2017].

[32] S. Patra, S. M. Hasan, N. Narasaiah and D. Chakrabarti, “Effect of bimodal distribution in ferrite grain sizes on the tensile properties of low-carbon steels,” *Materials Science and Engineering A,* no. 538, pp. 145-155, 2012.

List of Tables

Table 1: Oven- to sample-temperature calibration. 19

Table 2: Temperature ranges for the different functions. 20

Table 3: Temperature conversion factors for Experiment 1. 20

Table 4: Temperature conversion factors for Experiment 2. 21

Table 5: Average grain diameters for different soak temperatures at different times for Experiment 1. 26

Table 6: Average grain diameters for different soak temperatures at different times for Experiment 2. 26

Table 7: Average grain diameters for different soak temperatures at different times. 37

List of Figures

Fig. 1: Required steel type based on CO_2 and H_2S concentrations. 5

Fig. 2: Schematic set up of the HT-LSCM 8

Fig. 3: Grain boundaring grooving [23] 9

Fig. 4: Schematic diagram of the specimen geometry and the laser ultrasonics experimental set-up [3]. 10

Fig. 5: Pressure losses in a gas pipeline system with 4 compressor stations. 11

Fig. 6: Comparable Specific Transportation cost for 56" gas pipeline X80 [5] 13

Fig. 7: Relative comparison of specific transportation cost for gas pipeline systems (steel grade X70, max. operating pressure 91 bar abs.) [26] 14

Fig. 8: Relative comparison of specific transportation cost for gas pipeline systems (steel grade X80, max. operating pressure 141 bar abs.) [26] 14

Fig. 9: Temperature profile of the samples at different soak temperatures (1050°C, 1150°C, 1250°C) 16

Fig. 10: Grain size distribution of the sample heated to 1050°C after $t_{1,1050}$ = 180.07 s. 17

Fig. 11: Grain size distribution of the sample heated to 1050°C after $t_{2,1050}$= 242.78s. 17

Fig. 12: Grain size distribution of the sample heated to 1150°C after $t_{1,1150}$ = 94.84 s. 18

Fig. 13: Grain size distribution of the sample heated to 1150°C after $t_{2,1150}$ = 257.28 s. 18

Fig. 14: Grain size distribution of the sample heated to 1250°C after t = 66.23 s. 18

Fig. 15: Grain size distribution of the sample heated to 1250°C after t = 183.64 s. 18

Fig. 16: Sample from Experiment 1 heated up to 1050°C. 22

Fig. 17: Sample from Experiment 2 heated up to 1050°C. 22

Fig. 18: Sample from Experiment 1 heated up to 1150°C. 22

Fig. 19: Sample from Experiment 2 heated up to 1150°C. 22

Fig. 20: Sample from Experiment 1 heated up to 1250°C. 23

Fig. 21: Sample from Experiment 2 heated up to 1250°C. 23

Fig. 22: Dual stage heating temperature profile with 2 points of investigation. 24

Fig. 23: Evaluation of grain size distribution at t_2 (1050°C). 27

Fig. 24: 50 sections histogram at t_2 = 241.08 s (1050°C). 27

Fig. 25: Evaluation of grain size distribution at t_2 (1050°C). 27

Fig. 26: 50 sections histogram at t_2 = 242.78 s (1050°C). 27

Fig. 27: Evaluation of grain size distribution at t_2 (1150°C). 28

Fig. 28: 50 sections histogram at t_2 = 240.2 s (1150°C). 28

Fig. 29: Evaluation of grain size distribution at t_1 (1150°C). 29
Fig. 30: 50 sections histogram at t_1= 94.84 s (1150°C). 29
Fig. 31: Evaluation of grain size distribution at t_2 (1150°C). 29
Fig. 32: 50 sections histogram at t_2 = 257.28 s (1150°C). 29
Fig. 33: Evaluation of grain size distribution at t_2 (1250°C). 30
Fig. 34: 50 sections histogram at t_2 = 252.2 s (1250°C). 30
Fig. 35: Evaluation of grain size distribution at t_2 (1250°C). 30
Fig. 36: 50 sections histogram at t_2 = 270.91 s (1250°C). 30
Fig. 37: Summary of gained average grain sizes for the isothermal holding experiments. 31
Fig. 38: Evaluation of grain size distribution (1005.5°C)....31
Fig. 39: 25 sections histogram after 187.4 s (1005.5°C). 31
Fig. 40: Evaluation of grain size distribution (1251.2°C)....32
Fig. 41: 25 sections histogram after 478.3 s (1251.2°C). 32
Fig. 42: Resulting LUT average area weighted grain sizes over time. Time zero corresponds to 900°C 32
Fig. 43: Number weighted grain size distribution for 1050°C soak temperature at t_2. 34
Fig. 44: Area weighted grain size distribution for 1050°C soak temperature at t_2. 34
Fig. 45: Number weighted grain size distribution for 1150°C soak temperature at t_1. 34
Fig. 46: Area weighted grain size distribution for 1150°C soak temperature at t_1. 34
Fig. 47: Number weighted grain size distribution for 1150°C soak temperature at t_2. 35
Fig. 48: Area weighted grain size distribution for 1150°C soak temperature at t_2. 35
Fig. 49: Number weighted grain size distribution for 1250°C soak temperature at t_2. 35
Fig. 50: Area weighted grain size distribution for 1250°C soak temperature at t_2. 35
Fig. 51: Motion of triple junctions. 37
Fig. 52: Comparison between average area-weighted LUT and HT-LSCM grain size measurements. 38

Abbreviations

ASTM	American Society for Testing and Materials
CAPEX	Capital expenditure
CCD	Charge-coupled device
°C	Degree Celsius
d	Diameter
GUI	Graphical user interface
HAZ	Heat affected zone
HT - LSCM	High temperature laser scanning confocal microscopy & microscope
K	Kelvin
LUMET	Laser ultrasonics methodology
LUT	Laser ultrasonics technique
µm	Micrometer
OPEX	Operational expenditure
s	Seconds
t	Time